

WORCESTER POLYTECHNIC INSTITUTE

Ocean Wave Energy Harvesting

Off-Shore Overtopping Design

Steven Como, Passe Meas, Kelsey Stergiou, and Jessica Williams

With the Assistance of Jan Keleher
4/30/2015

This report represents the work of WPI undergraduate students submitted to the faculty as evidence of completion of a degree requirement. WPI routinely publishes these reports on its website without editorial or peer review. For more information about the projects program at WPI, please see <http://www.wpi.edu/academics/ugradstudies/project-learning.html>

Abstract

Renewable energy is a constantly discussed topic in the scientific world, for many of the energy sources used daily are in short supply. As the ocean makes up 70% of the Earth, wave energy is an option that could potentially produce a large amount of power. Various wave-capturing mechanisms were researched and analyzed. A new device was designed and manufactured, while a wave tank was constructed to test the power output of the device. By simulating deep water waves, it was found that the power produced by the prototype yielded approximately 0.010W. Using Froude scaling ratios, a scaled up model would produce about 254 W/ft of wave front. This power production compares to similar devices at about 133 W/ft; however the overall size of the new device is much smaller than the massive scale of competing products. The proposed design defines a space-efficient model for producing sustainable energy from wave power.

Table of Contents

Abstract	i
Table of Figures	iii
Table of Tables	iv
Chapter 1 – Introduction	1
Chapter 2 – Background	2
2.1 Why Renewable Ocean Energy?	2
2.2 Why Waves?	2
2.3 Types of Wave Energy Harvesting	6
2.4 Overtopping Design Combination	8
Chapter 3 - Methodology	11
3.1 Existing Designs.....	11
3.2 Scaling Factors	11
3.2.1. Assumptions	12
3.2.2. Froude Scaling Factor.....	13
3.2.3. Power Calculations	16
3.3 Development of Wave Generation System	18
3.3.1. Wave Height Calculations	19
3.3.2. Geometry of Four Bar Mechanism.....	22
3.3.3. Power Requirements & Motor Preparation	23
3.3.4. Stresses Exerted at the Joints.....	30
3.3.5. Other Considerations	32
3.4 Design of Overtopping Device.....	33
3.5 Construction of Test Tank and Device.....	36
3.5.1. Test Tank Construction	36
3.5.2. Device Construction	37
3.5.3. Assembly of Testing Unit.....	38
Chapter 4 – Testing & Data Collection.....	42
Chapter 5 – Results & Analysis	45
Chapter 6 – Conclusions & Future Improvements	51
References.....	52
Appendix A.....	54

Table of Figures

Figure 1: Map of Wave Power Potential throughout the World.....	2
Figure 2: Schematic Deriving Potential Energy and Power of a Wave	5
Figure 3: Point Absorber Device	6
Figure 4: Wave Attenuator Device	7
Figure 5: Oscillating Water Column.....	8
Figure 6: Overtopping Device	8
Figure 7: Schematic of Device.....	16
Figure 8: Wave Capture Schematic	17
Figure 9: Wave Generation Mechanism	19
Figure 10: Diagram for Wave Height Determination	21
Figure 11: Wave Generator Geometry.....	23
Figure 12: FBD of Board	24
Figure 13: FBD of Rod	25
Figure 14: FBD of Cam	26
Figure 15: Variety of Duty Cycle Outputs Generated by PWM.....	27
Figure 16: Circuit Diagram of Pulse Width Modulator	28
Figure 17: Motor Cam	29
Figure 18: Cam Attached to Motor.....	29
Figure 19: Hinges Connecting Board to Test Tank	30
Figure 20: Pin Connecting Rod to Board.....	31
Figure 21: Pin Connecting Cam to Rod.....	32
Figure 22: Overtopping Prototype	33
Figure 23: Ramp Design	34
Figure 24: Tier Section Design	35
Figure 25: Tier Drain System	35
Figure 26: SolidWorks Drawing and Model of Wave Tank.....	36
Figure 27: Exploded View and Final Construction of the Wave Tank.....	36
Figure 28: Biscuit Joint Exploded View	37
Figure 29: Clamped Tier 1 to Allow Proper Setting Of Biscuit Joints.....	37
Figure 30: Cross-Section of the Sideboards.....	38
Figure 31: SolidWorks Drawing of the Backboard	38
Figure 32: Drawing of Expansion Adapter for Water Collection.....	39
Figure 33: Inner Tube Design for Testing Different Tiers	39
Figure 34: Finalized Inner Tube Design with O-Rings	40
Figure 35: Final Assembly Wave Generator	41
Figure 36: Final Assembly Wave Converter	41
Figure 37: Characteristic Waves	42
Figure 38: Low-Head Kaplan Turbine Characteristics.....	49

Table of Tables

Table 1: Froude Scaling Ratio for Model and Prototype Similarities	14
Table 2: Froude Scaling Ratios for Model Scaling.....	15
Table 4: Volume Collection Data	43
Table 5: Drain Time and Volumetric Flowrate.....	44
Table 6: Prototype Scale Power Output.....	46
Table 7: Froude Scaling Ratio Calculations	47
Table 8: Full-Size Model Scale Power Output	47
Table 9: Low-Head Kaplan Hydro Turbine Specifications	47
Table 10: Low-Head Kaplan Turbine Calculations	48
Table 11: Optimized Number of Kaplan Turbines	50
Table 12: Actual Power Output of the Full-Scale System.....	50
Table 13: Proposed Design vs. Existing Market.....	50

Chapter 1 – Introduction

The population is well aware of the energy crisis and the need for clean, renewable energy sources. Due to the high potential of ocean power available in waves, wave energy harvesting is an industry with a constant flux of emerging start-up companies innovating ideas to capture this energy. Waves are a natural, renewable, free source of energy, providing an ideal alternative to other detrimental sources because the collection and redistribution of waves allows for endless energy harvesting. Through many approaches in converting wave energy into electricity, cost efficiency, safety, and reliability have been defining features of success. There are four main types of energy converter mechanisms, but overtopping devices will be the focus for this project.

Overtopping devices collect ocean waves in an above-water reservoir and then discharge the water into the ocean by means of turbines. The Wave Dragon is an example of an overtopping device that gathers waves by using two long arms that direct water into a central reservoir. The Wave Dragon then releases the water back into the ocean once it has gone through the turbines. The Seawave Slot-cone Generator utilizes tiered reservoirs to amass more of the wave without using arms to reroute it. Within this project, a three-tiered overtopping device was developed to collect waves of differing heights within a motorized wave tank that would simulate deep-water waves. The deep-water aspect of the device appeals to the aesthetic dimension, for a coastal collection overtopping device impedes the view from beaches and coastlines. It can also upset fishing locations and habitats of a variety of sea creatures. This new overtopping device was a combination of many ideal characteristics of other researched wave harvesting devices, including the tiers and turbines to collect the waves and produce power. Many calculations were performed to discover the ideal scaling factors, proper cam dimensions, and necessary motor parameters. The purpose of this project was to develop a new overtopping device that could produce just as much power, if not more, than products currently on the market.

Chapter 2 – Background

2.1 Why Renewable Ocean Energy?

The need for additional energy to sustain the growing population of the world calls for better and more innovative technologies. Many current technologies include nuclear power or biofuels, which have been linked to environmental concerns. Ocean energy harvesting devices became popular in 2008 with an array of designs, including floating wind turbines, as well as tidal, wave, and thermal energy converters (Esteban, 2012). Clean, renewable energy harvesting is preferred over nuclear or biofuel-powered plants, but many renewable sources are unable to be operated on a large-scale. In order to find a way to implement large-scale operation, different designs are continuously being researched and developed.

2.2 Why Waves?

The advantages of wave energy harvesters outnumber the advantages of other ocean energy harvesting methods such as tidal power, ocean thermal energy conversion (OTEC), and saline mechanisms. Waves are abundant in all areas throughout the ocean, making them more useful in energy harvesting than tides. Although tides have the potential to generate large amounts of power (approximately 3,000 GW worldwide) less than 3% of areas are suitable to actually harness tidal power (Esteban, 2012). Tides are predictable and consistent; however, due to the limited abundance of locations, tidal power is difficult to incorporate on a large scale. Alternatively, waves are not as easy to predict, but they are found in many more locations throughout the world, as can be seen in Figure 1.

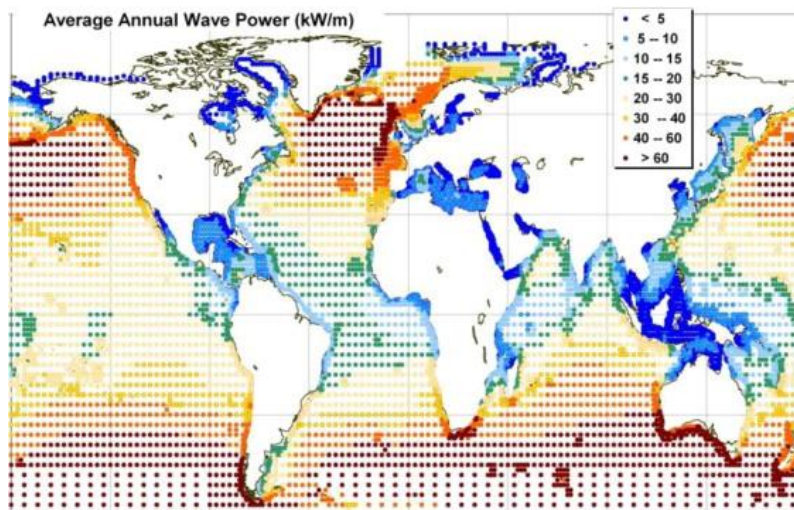


Figure 1: Map of Wave Power Potential throughout the World (Alamian, 2014)

The map shows that there is high wave power potential in widespread areas, especially those further from the equator. Wave energy has been estimated to have the potential to produce 1,000-10,000 GW of power, which is close to the world electrical energy consumption (Esteban, 2012). From this information, it can be argued that wave energy harvesting is more accessible than tidal energy harvesting.

Although wave energy converters provide a method for clean energy harvesting, there are some disadvantages in using this technology. A primary concern of implementing any mechanical device into the marine environment is the potential of polluting the water. This pollution may be in the form of debris, oil, or other lubricants from the device. To ensure the cleanliness of the proposed design, the electrical generator is located onshore and underwater power lines will allow associated components to be located on land. Furthermore, imposing on natural habitats is an environmental hazard presented by construction of any systems. Since the device floats on the water in the open ocean, no habitats will be disturbed and any harm to animals would be very unlikely. Lastly, invasive products introduced into the environment are aesthetically deterring to tourists and natives of the region. Wave energy converters are massive and can take away from the natural beauty of the marine atmosphere. The proposed system addresses this issue by the utilization of open ocean waves and locating the device out of sight and therefore out of mind. In conclusion, the disadvantages that generally result from such devices were accounted for in the design to best suit the environment.

Another form of ocean energy harvesting is by OTEC mechanisms. OTEC utilizes the ocean's natural absorption of solar energy to produce power. As the heat of the sun warms the surface of the water a temperature gradient is created. The temperature of the surface water will vaporize a fluid with a low-boiling point, which will then expand into gas and spin a turbine. This turbine is connected to a generator, which produces electricity. Cooler seawater is brought in by a pump that cools the vapor back into a liquid so it can be continuously reused in the cycle. The larger the temperature differential, the higher the efficiency of the cycle; therefore, ideal locations for this technology include waters around the Equator (Esteban, 2012). The limitation of efficiency and location provides evidence why waves are a more accessible and favorable option in the field of ocean energy harvesting.

Prototype saline mechanisms harvest energy from bodies of water where both fresh and salt water are present, such as estuaries. The mechanism divides the water types by means of a

semipermeable membrane. The osmosis that occurs as the fresh water moves across the gradient of higher salinity to dilute the solution increases pressure. Once the system reaches a certain pressure, achieving a high enough head, it will spin a turbine and generate power (Lockwood, 2013). The complexity of this mechanism, along with the limitations in location, makes saline energy converters less feasible than wave energy converters.

Although a number of renewable energy sources are undergoing research, wave energy harvesting provides advantages over other competitive methods. One major advantage is the wide span of locations in which waves can be captured. Devices can be incorporated in the open ocean where high energy waves are present or along the coastline to minimize construction and maintenance costs. Unlike solar energy, waves can be continuously collected at all hours of the day and night. In addition to the versatility in location and collection times, waves are produced year round and are a source of free energy. A major benefit of wave converter devices is their minimal use of land when compared to wind farms, power plants, and other power production sites such as the Alaskan pipeline. There are numerous advantages to using different forms of alternative energy; however, wave power is a compelling source for energy production.

In order to understand how to extract power from waves, it is essential to first understand the mechanism of how waves work. Waves are created by the force of wind on open water. As the force of the wind reaches the surface of the water, waves are produced. These waves then travel, containing high amounts of energy, until they reach an area of shallow depth, usually a beach. At this point, waves begin to lose energy due to frictional losses at the seabed surface. The wavelengths shorten, speeds are reduced, and the wave profile steepens; resulting in the “breaking” of the wave (Tester, 2012). Due to this loss of energy, waves in open water have much higher energies than waves that are found along coastal regions.

All waves have potential energy that can be transformed to power through use of wave energy converters. Waves that are far offshore exhibit higher potential energy than waves that are found near the shoreline by about 10% (Thurman, 2001). The potential energy of a wave can be calculated by the following equation:

$$\Delta PE = \frac{1}{16} \rho \lambda g h^2$$

In this equation, the potential energy only accounts for two dimensions, meaning that this is the potential energy per unit width of the wave. The variables in the above equation represent:

$\rho = \text{density of the water } \left(1025 \frac{\text{kg}}{\text{m}^3} \text{ for seawater}\right)$

$g = \text{acceleration of gravity } \left(9.81 \frac{\text{m}}{\text{s}^2}\right)$

$h = \text{crest - to - trough wave height (about 2m)}$

$\lambda = \text{wavelength}$

The wavelength can be described as:

$$\lambda = \frac{gT^2}{2\pi}$$

Where:

$T = \text{wave period (approximately 5 - 10s)}$

The potential energy of the wave can then be converted to power by dividing the potential energy by the time period. This results in the following equation for power:

$$P = \frac{1}{32\pi} \rho g^2 h^2 T$$

Substituting the density of seawater (1025 kg/m^3) and acceleration due to gravity (9.81 m/s^2) into the equation, it can be reduced to:

$$P = 0.98h^2T$$

The units for this power equation are kW/m, meaning that the result gives the power output per unit width. For comparison, the Wave Dragon produces a range of .4 kW/m for the smallest model and about 48kW/m in its largest design. A schematic of a wave is shown in Figure 2.

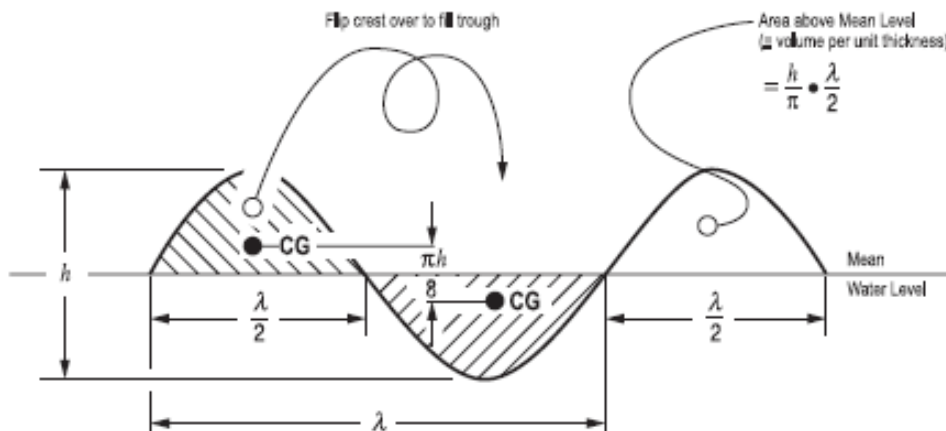


Figure 2: Schematic Deriving Potential Energy and Power of a Wave (Tester, 2012)

This schematic includes variables that are used to derive the potential energy and power equations for a wave. From this, one can better understand the mechanics of a wave and therefore predict the power output for a wave energy converter.

2.3 Types of Wave Energy Harvesting

There are numerous devices that have been established in the wave energy industry that attempt to most efficiently convert the potential energy of waves into power. The four primary categories of wave energy converters (WECs) are: point absorbers, attenuators, oscillating water columns, and overtopping devices. Each of these WECs has different attributes, all with varying advantages and disadvantages.

Point absorbers, seen in Figure 3, are the simplest WECs. These devices float on the surface of the water and generate energy through the periodic passing of waves, causing the device to bob up and down. Point absorbers depend on an internal hydraulic system that pumps air to power a generator as the cylinder is compressed and released by wave energy. They rely on the frequency of waves to generate electricity and can attain maximum energy absorption by matching the optimal frequency and wave height (Voorhis, 2012). The disadvantages of point absorbers are their inability to adapt to the varying height and frequency of waves, which prevents optimization through consistency. Additionally, large waves produced by storms significantly reduce the efficiency of these devices and can even damage them if they are too forceful.



Figure 3: Point Absorber Device (Voorhis, 2012)

Attenuators are long, cylindrical, segmented structures that float on the surface of the water, operating in parallel with the roll of the waves, much like the motion of a ship. The segmented regions allow for these cylinders to bob in the water due to passing waves which drive the hydraulics of the device similar to that of point absorbers. The difference between attenuators and point absorbers rests primarily in the relative size of the structures. The mechanics of the two systems operate on similar basic principles of hydraulics driven by periodic wave frequencies; however, the attenuators are able to capture a wider range of waves due to their large size. Additionally, attenuators are more rugged, as can be seen in Figure 4 below, and can survive harsh storms that generate greater waves.



Figure 4: Wave Attenuator Device (Pelamis, 2012)

Oscillating water columns operate based on a pressure differential created between air and the ocean water within a structure that is partially submerged. These columns are constructed along the shoreline to capture waves crashing on the coast, utilizing the wave pressure to push air through a hollow cavity that is attached to a turbine. The rapid decrease in water pressure then pulls air back through the bi-directional turbine, generating electricity through air flow in both directions. This structure provides a simple, sturdy design that is able to convert wave energy at low maintenance costs due to the lack of complex internal machines. Although costs are saved by building the structure into the shoreline, many marine habitats are located along the coast. Consequently, implementing devices on the shoreline has larger environmental implications than open ocean devices. An example of an oscillating water column can be seen in Figure 5 below.

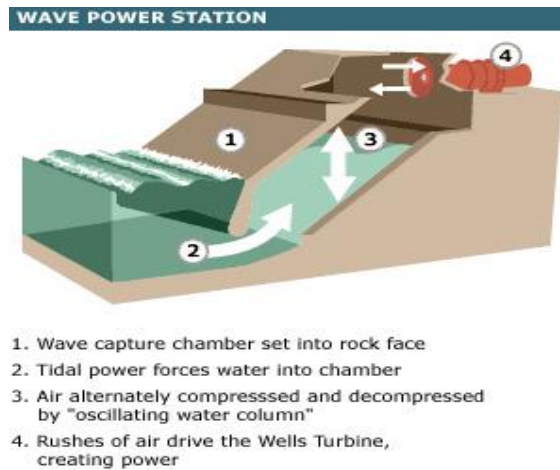


Figure 5: Oscillating Water Column (Emay, 2010)

Lastly, overtopping devices function based on a pressure differential created between an artificial reservoir and the surrounding ocean water. The basic design of overtopping devices involves a ramp leading up to a reservoir with a retaining wall. Potential energy is then converted into power through turbines that are located in the bottom of the reservoir as shown in Figure 6. The water level rises within the reservoir as waves crash over the ramp, creating a pressure gradient. As a result, the generated head forces water out through the turbines within the structure. Compared to oscillating water columns, this straightforward, robust design provides a means for capturing a large volume of waves and generating electricity without the use of internal mechanisms, therefore minimizing the cost of maintenance and repair.

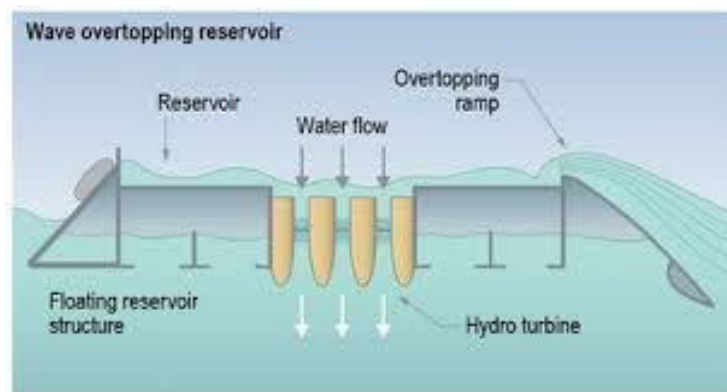


Figure 6: Overtopping Device (Bedard, 2005)

2.4 Overtopping Design Combination

By researching various methods in wave energy conversion, a new device that combines the advantages of overtopping with a multi-tiered system was conceptualized. With a rapidly expanding market for WECs, numerous innovations exist; however, there is great potential to

create more efficient designs to produce free energy. By combining ideas from two pre-existing designs, the Seawave Slot-cone Generator and Wave Dragon, a new overtopping system was created.

The Seawave Slot-cone Generator (SSG) is an overtopping device that was created by WAVEenergy in Norway. The SSG utilizes multiple tiers that store the energy of collected waves until it can be converted into electricity through a multi-stage turbine. Compared to similar water collection devices, the SSG has added effectiveness due to its multiple reservoirs, higher cost-efficiency due to incorporation into pre-existing structures, water recirculation, and easy installation/maintenance due to the fact that no cables or moorings need to be mounted underwater. A disadvantage of the SSG falls within its location. Since it is used along the coast, the size of the waves that it encounters is smaller due to shoreline frictional effects, and therefore less powerful than those of systems that are installed offshore. In terms of economic and technical dilemmas, there have been some questions related to the protection of harbors if the SSG is assimilated into pre-existing structures (Vicinanza, 2012).

Erik Friis-Madsen and Wave Dragon Ltd. invented and developed the Wave Dragon. This overtopping device floats on top of the water and collects waves by means of two large arms, known as wave reflectors. These reflectors direct waves towards a ramp where they crash into a reservoir. The water is then briefly stored before leaving the reservoir through Kaplan turbines located at the bottom. Kaplan turbines are usually used in hydropower plants as they produce electricity from hydraulic head. The water is returned to the ocean after it runs through the turbines and this constant cycle creates a clean source of energy that can be reused indefinitely. “Wave Dragon is currently the largest device – by rated power and physical dimensions – under development” (Wave Dragon, 2006). In 2003, the first power-collecting prototype of Wave Dragon was set up at Nissum Bredning, which is off the coast of Denmark. The energy production of this device is constant, with an annual energy output of about 619 MWh. The system has a capacity factor of approximately 20%, and can be downsized to collect the energy from smaller waves as well. Wave Dragon is unable to produce electricity from waves with heights of less than 1 m, as well as in cases with overly large waves, such as a tropical storm or a tsunami. The device is designed to handle “energetic wave climates”, which is defined as areas where the wave power density is 50 kW/m or higher (Wave Dragon, 2006).

Combining the onshore, multi-tiered, SSG with the popular Wave Dragon provides a wide range of benefits to improve the power output of the design. A primary advantage of utilizing the open ocean versus a shoreline device is the difference in energy capacity for the characteristic waves. Open ocean waves contain approximately 10% more power than shoreline waves due to the frictional losses of the ocean floor. These losses act on waves shallower than one half of the wavelength deep, which is the case for the majority of waves crashing on shore. The effective depth of the wave is equal to about one half of the wavelength; therefore, in shallow waters, the ocean floor actually opposes wave movement, reducing the overall energy of the wave (Vicinanza, 2012).

A major downfall of the Wave Dragon design can be attributed to the limited capture of waves at specific heights dependent on the ramp of the device. The Wave Dragon limits collection based on a set height for the ramp, reservoir, and external walls, whereas the multi-tiered on-shore device captures waves at varying heights. Potential energy relies on the height at which the wave is captured and is maximized at the highest point of the wave. By capturing the wave at its tallest height, the maximum potential energy of the wave may be collected by the system. Since the system can also accept waves shorter than the maximum height, the conceptual combined design optimizes the heights and volumes of capture for improved reservoir efficiencies.

Furthermore, the reservoir draining of the Wave Dragon produces additional inefficiencies by starting and stopping the turbines in the system as each cycle of water empties out. By using a multi-tiered system, there is a higher possibility of maintaining a larger volume of water in the reservoirs to establish constant flow through the turbines. This achievement will significantly improve the efficiency of the system by drastically reducing frictional losses in the turbines. This reduction in losses results from preventing the stopping and starting inefficiencies of the turbines from occurring at each wave cycle and keeping the turbines in constant motion. Since the multi-tiered system captures waves at different levels and fills multiple reservoirs, the water takes longer to drain through the system, thus providing constant head to keep the turbines spinning.

Chapter 3 - Methodology

The goal of this project was to test and compare the power output produced by combining two overtopping designs, Wave Dragon and SSG, into one wave energy harvesting device. To achieve this goal, the following objectives were completed:

1. Conducted research on Wave Dragon and Seawave Slot-cone Generator to determine which characteristics were most favorable at producing high wave energy efficiencies.
2. Used proper scaling factors to determine reasonable testing conditions.
3. Researched, developed, and designed a wave generation system that produced the necessary testing environment.
4. Designed a model utilizing SolidWorks software of the intended overtopping device.
5. Constructed the test tank and wave energy converter.
6. Performed testing and gathered data on the power output of the new device.
7. Analyzed the power produced by the device.

This chapter contains descriptions of objectives 1-5 and methods used throughout the process that enabled the completion of the overall goal: comparing the power output of two overtopping designs.

3.1 Existing Designs

In order to develop a new overtopping device, existing designs were first explored. Two designs that exhibited high potential in the field of wave energy harvesting included Wave Dragon and SSG as discussed in Chapter 2. By combining the multiple reservoirs of SSG with the offshore aspect of Wave Dragon, the concept of a superior wave power generation device was fashioned.

3.2 Scaling Factors

In order to create a functional scale model of the wave energy converter, it was important to evaluate the feasibility of the presented design. Assumptions needed to be made regarding inefficiencies and losses that would be encountered during testing. These assumptions included the percentage of wave volume captured, efficiency of the turbines, and the efficiency of the generator. Considering the different inefficiencies and assumptions of the wave converter system, preliminary calculations gave more tangible parameters for the device as well as an estimate of the potential power output.

3.2.1. Assumptions

There are a number of assumptions to be considered when analyzing any power system. A full scale model of this overtopping device would consist of turbines and generators that would exhibit losses due to friction and inefficiencies. To simplify the prototype, a turbine and generator were omitted; however, the efficiency of these devices were considered when calculating the overall power output of the system. Researching current technology, revealed most hydraulic turbines and generators yield efficiencies ranging from 85% to 95%. Additionally, Froude scaling factors were calculated in order to relate the prototype to the full sized device. The basis for these scaling calculations was derived from the estimated wave height produced by the wave generation system. The combination of all of these assumptions provides a baseline for preliminary power calculations that the designed system can expect to produce.

Furthermore, when waves travel up the ramp into the reservoirs, the entirety of the wave will not be captured. For purposes of simplification, it was assumed that 75% of any given wave volume would be captured by the device based on wave geometry. Realistically, this value would change for each wave dependent on the wave height and other wave characteristics. In relation to wave volume captured, the “felt” wave height is important since waves do not solely act above the water. Research shows that the “felt” wave height extends approximately half of the wavelength below the surface of the water (Thurman, 2012). Considering this assumption was vital to the design of the system to assure that the test tank was deep enough to enable free movement of the effective depth of the wave. Assuming deep waves as opposed to shallow waves more accurately depicted the system on the open ocean because it neglected frictional losses of the ocean floor. Removing these frictional losses provides an advantage over a shoreline system.

The wave height was estimated under the assumption that the “felt” height extends half of the wavelength beneath the surface of the water. The wavelength was assumed to be seven times the chosen wave height as is the average characteristic of a general wave system (Thurman, 2012). Based on the wave height and wavelength assumptions the maximum “deep ocean” wave height was modeled using the following function:

$$h_{wave} = \frac{2}{7} * h_{water}$$

Where h_{wave} is wave height and h_{water} is the water height. Using the above equation prevents frictional losses from the bottom of the test tank, enabling open ocean waves to be simulated. Therefore the maximum potential wave height within our testing conditions is:

$$h_{\text{wave}} = \frac{2}{7} * 12 \text{ inches} = 3.43 \text{ inches} = 8.71 \text{ cm}$$

3.2.2. Froude Scaling Factor

Froude scaling factors are important dimensionless numbers to be considered when designing a system that involves wave production. Froude scaling is beneficial since the Reynolds number is a more difficult factor to scale. “If Re is ... kept constant, the value of U (velocity) at model scale has to be... that of the full-scale value. The obvious way to overcome these conflicting requirements would be to increase g and/or decrease ν (viscosity)” (Payne, 6). In order to achieve these conditions, a centrifuge or vacuum chamber would be required for testing. Both options were unfeasible within an undergraduate project constraint, so Froude scaling factors were used.

Froude scaling is more practical than Reynolds scaling. The Froude scaling factor can be derived from the similarity of Froude numbers for the system shown by:

$$F_M = \frac{V_M}{(g_M L_M)^{\frac{1}{2}}} = \frac{V_p}{(g_p L_p)^{\frac{1}{2}}} = F_p$$

Where F represents the Froude numbers for the model and prototype, V is the velocity, g defines the gravitational constant, and L resembles the characteristic length. Additionally, $g_M = g_p = g$ and $L_p = \lambda L_M$, where λ represents the wavelength. Substituting the gravity constant and geometrically similar factors this equation yields:

$$F_M = \frac{V_M}{(g L_M)^{\frac{1}{2}}} = \frac{V_p}{(g \lambda L_M)^{\frac{1}{2}}} = F_p$$

Which then reduces to:

$$V_p = \lambda^{1/2} V_M$$

From this derivation, it can be seen that the scale ratio required to upscale Froude model velocities is $\lambda^{1/2}$. Additional derivations can be completed in a similar manner to calculate the Froude scaling factors for other variables shown in Table 1.

Table 1: Froude Scaling Ratio for Model and Prototype Similarities

Parameter	Dimension	Froude	Reynolds
Geometric similarity			
Length	[L]	λ	λ
Area	[L ²]	λ^2	λ^2
Volume	[L ³]	λ^3	λ^3
Rotation	[-]	1	1
Kinematic similarity			
Time	[T]	$\lambda^{1/2}$	λ^2
Velocity	[LT ⁻¹]	$\lambda^{1/2}$	λ^{-1}
Acceleration	[LT ⁻²]	1	λ^{-3}
Discharge	[L ³ T ⁻¹]	$\lambda^{5/2}$	λ
Dynamic similarity			
Mass	[M]	λ^3	λ^3
Force	[MLT ⁻²]	λ^3	1
Pressure and stress	[ML ⁻¹ T ⁻²]	λ	λ^{-2}
Energy and work	[ML ² L ⁻²]	λ^4	λ
Power	[ML ² T ⁻³]	$\lambda^{7/2}$	λ^{-1}

The various scaling factors account for the wave conditions that vary based on geometric, kinematic, and dynamic similarities. The similarities between the prototype and the full-scale model allow for the proper extrapolation of data from experimental testing. Table 1 can be used to determine a wave period and frequency based on the wave height derived for the system. Additionally, the mass of the waves captured and the power potential of the waves can be estimated by using these scaling factors.

Given the wave height of 3.43 inches (8.71 cm), the wave period can be scaled appropriately by the Froude scaling factor of $\lambda^{0.5}$, where λ is equal to the wave height. Therefore, the scaling factor for the period associated with the given wave height is:

$$\lambda_M = \lambda_p^{0.5} = .0871^{0.5} = 0.295$$

Where λ_M is the Froude scaling factor for the wave period given a wave height of 3.43 inches. Multiplying this scale factor by an average period of ground swell waves, which characterize the waves acting in deep ocean water, yields:

$$T = \lambda_M * 9s = 0.295 * 9s = 2.66 s$$

Where T is the scaled period of the waves given a 3.43 inch wave height and 9 seconds as the average period for ground swell waves for a full-scale system. Therefore a reasonable scale for the wave period based on a 9 second ground swell period is approximately 2.66 seconds.

Using a similar method, the mass and power potential for each wave can be estimated based on the various Froude scaling factors that are derived from the table above. The mass of each wave captured by the wave converter can be estimated by:

$$\lambda_M = \lambda_p^3 = .0871^3 = 6.61 \times 10^{-4}$$

Where λ_M is the Froude scaling factor for the mass of each wave for the full-scale system in relation to a 3.43 inch wave height produced. To find the actual mass captured by each wave, the scaling factor can be multiplied by the estimated mass for a full scale system.

Finally, the same method can be utilized substituting λ^3 with $\lambda^{3.5}$ to estimate the power of the scaled system based on the full size system. The power scaling coefficient will then be calculated by:

$$\lambda_M = \lambda^{3.5} = .0871^{3.5} = 1.95 \times 10^{-4}$$

Where λ_M is the Froude scaling factor for the power potential of each wave of the full-scale model compared to that for the 3.43 inch wave height. Again, the actual power potential for each wave for the scaled system can be achieved by multiplying this scaling factor by the estimated power in a life sized system. The results for each scaled variable are calculated in a similar manner and the important kinematic and dynamic similarities are displayed in **Error! Reference source not found.** below.

Table 2: Froude Scaling Ratios for Model Scaling

Parameter	Dimension	Froude Scaling Ratio
Time	[T]	0.295
Velocity	[LT ⁻¹]	0.295
Acceleration	[LT ⁻²]	1
Mass	[M]	0.000661
Force	[MLT ⁻²]	0.000661
Pressure and Stress	[ML ⁻¹ T ⁻²]	0.0871
Energy and Work	[ML ² T ⁻²]	0.0000576
Power	[ML ² T ⁻³]	0.000195

Froude scaling factors can be used for a variety of assumptions by simply defining a wave height. In using these scaling factors, the accuracy of the power calculations can be

determined. These values can be further compared to experimental data to estimate losses for the designed system.

3.2.3. Power Calculations

In order to ensure the feasibility of the device, it was necessary to complete some of the background theoretical power calculations. These calculations involved the scaling factors derived above, the specific design of the wave capture device, and the volume and potential energy of water in the reservoirs.

The new design uses three separate tiers to capture water. The collection of water at its peak height stores the highest potential energy of the wave. Due to the shape of each wave (the wavelength being approximately 7 times the height of the wave), the first tier is designed to capture as much water as possible from the lower part of the wave. The second and third tiers are designed to optimize wave collection at the wave's maximum height. All the reservoirs and tiers are lipped so that any excess water from the higher tiers will simply flow down to the tier below it.

The tiers are designed for a maximum height equal to 1.2 times the average wave height. This allows for the maximum capture of over 95% of waves, and allows for the device to utilize the forward kinetic energy of the waves to bring them up the ramp, to a higher reservoir, maximizing potential energy. The schematic in Figure 7 shows how the wave is split into three tiers correlating to the three tiers of the device.

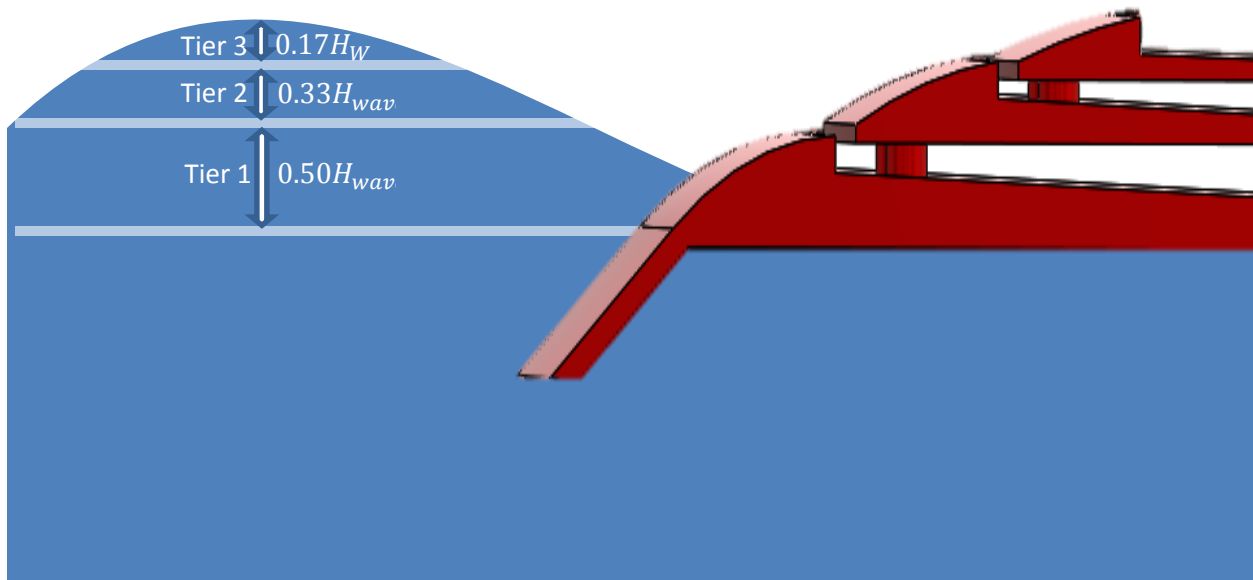


Figure 7: Schematic of Device

It was previously determined that the simulation tank, containing a water depth of 12 inches (or 0.305 meters), is able to produce 3.43 inch waves. Using 3.43 inch simulated waves, estimation of the wave collection capacity and the power output of the testing device was determined. Deep ocean waves generally have the following relation between wavelength and wave height:

$$\text{Wavelength of Wave} = \lambda = 7h$$

As such, borrowing the relation for the area of a wave given in Figure 2 also provides the following equation for the Area of a wave.

$$\text{Area of a Wave} = \frac{h}{\pi} * \frac{\lambda}{2} = \frac{h}{\pi} * \frac{7h}{2} = \frac{7h^2}{2\pi}$$

From this relation it is possible to divide the total area of the wave into sections that would enter the three tiers separately, optimizing the potential energy.

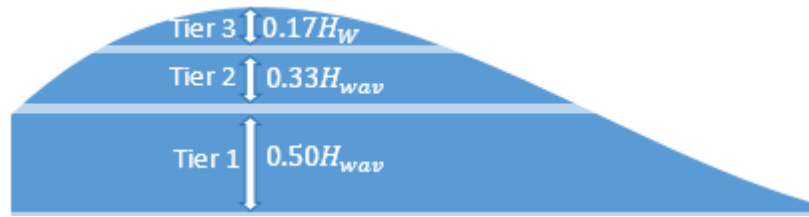


Figure 8: Wave Capture Schematic

It is possible to determine the area of each tier separately by using the equation for the area of the wave. The area of tier 3 represents a sixth (0.17) of the total wave area, therefore the height must be also be divided by 6. The sum of tiers 2 and 3 represent half of the total wave height and to find the area of tier 2, the area of tier 3 is subtracted. Finally, to find the area of tier 1, a similar approach is taken. The area of tiers 2 and 3 are subtracted from the total area of the wave to find the area of tier 1.

$$\text{Area of Tier 3} = T_3 = \frac{h \lambda}{2\pi} = \frac{7h^2}{2\pi} = \frac{7h^2}{6} = 2.18 \text{ in}^2$$

$$\text{Area of Tier 2} = T_2 = \frac{h \lambda}{2\pi} - T_3 = \frac{7h^2}{2\pi} - T_3 = \frac{7h^2}{2} - T_3 = 4.37 \text{ in}^2$$

$$\text{Area of Tier 1} = T_1 = \frac{h \lambda}{2\pi} - T_2 - T_3 = \frac{7h^2}{2\pi} - T_2 - T_3 = \frac{7(h^2)}{2\pi} (0.75) - T_2 - T_3 = 6.56 \text{ in}^2$$

Calculations of volume, energy and power values are “per inch” for the width of the device. Instead of considering the volume of each wave, the area of each wave (or volume per inch) will be considered. In addition, most of the calculations will remain as per wave values. The total captured volume (per inch), is a summation of the volume captured in each tier.

$$Total \frac{Volume}{inch} \text{ of All Tiers} = T_T = 13.1 \text{ in}^2$$

From the volume captured in each reservoir height, the potential energy stored in each reservoir was extracted. Simply put:

$$PE = mgh = V\rho gh$$

$$PE_{Total} = \rho g(V_1 h_1 + V_2 h_2 + V_3 h_3) = 1.52 \text{ Joules}$$

This is per wave per inch of device structure, therefore the power output can be estimated under the assumption that the volumetric flowrate in is equal to the volumetric flowrate out. It was assumed that the flowrate is constant, meaning that the reservoirs are replenished every wave period of 3 seconds. As such:

$$Power = \frac{PE_{Total}}{T} = \frac{1.52}{3} = 0.51 \text{ Watts}$$

Using the scaling factor derived from the Froude Number of $\lambda^{3.5}$, this gives us a real world output of about 2.6 kW per wave per meter of the device. This power output was calculated using 3.43 inch waves and tier heights based off this value. Therefore the wave capture efficiency was maximized for these ideal conditions.

3.3 Development of Wave Generation System

Once the appropriate scale for the prototype and waves was determined, a wave generation system was developed in order to test the prototype. This design utilized a crank-rocker four-bar mechanism. In this mechanism, a 24-inch plywood board was hinged to the bottom of a test tank to act as a rocker. At the top of the board, a rod was attached by a pin. The rod can be modeled as a two-force member, with only the force of the board and the force of the other linkage acting on it. The end of the rod opposite the board is pinned to a cam that is press-fitted on a motor shaft, which acts as the crank. A picture of the four bar mechanism can be seen in Figure 9.

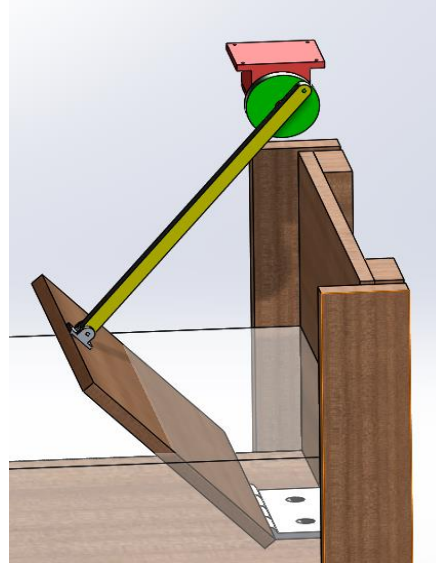


Figure 9: Wave Generation Mechanism

In order for a four bar linkage to have a link that can complete a full revolution, Grashof's condition must be satisfied. Grashof's condition states that the sum of the lengths of the shortest and longest links must be less than the sum of the lengths of the two intermediate-sized links (Natesan, 1994). In a traditional four bar linkage, there are additional limitations to the lengths of the bars to avoid locking of the mechanism, but these limits can be ignored since the crank and rocker are on two completely different planes. In this system, the concern is not centered about locking out the mechanism, but rather ensuring that the links are long enough for all ranges of movement.

As the board rocks back and forth, the water is displaced and waves are created. The height of the waves and the frequency of wave production can be adjusted by changing the geometry of each of the links, the mass of the board, and the power of the motor. Additionally, changing the position of the rocker relative to the crank alters the board angle, which generates waves of different heights. To ensure that the wave generation system produced the necessary testing environment, several aspects were considered: the water displacement and wave height, the geometry of the linkages, the power requirements and motor selection, and the stresses exerted at the joints. Other considerations were made to determine the proper features of the test tank, including material selection and placement of electronic equipment.

3.3.1. Wave Height Calculations

The first step to create the proper testing conditions was to calculate the wave heights that could be produced by this system. Since the movement of the board produces waves, the volume

of water that the board displaces should be equal to the volume of the wave. Making the mathematical assumption that the cross-sectional area of ocean waves can be modeled as two-dimensional sine waves, a sine function was generated. Knowing that the wave period is one wave every three seconds and that there is no horizontal or vertical shift, the amplitude, which in this case equals wave height (h_{wave}), is left as the only unknown.

$$h_{wave} * \sin\left(\frac{2\pi}{3}t\right)$$

Integrating this equation over the time interval of one wave results in the cross-sectional area of the wave. Taking this area and multiplying it by the width of the test tank gives the volume of the wave. Since the volume of displaced water is equal to the volume of the wave, the wave height can be easily calculated. To calculate this unknown, the cross sectional area of displaced water was divided by the integral of the wave during half of its time interval. This resulted in the following equation:

$$h_{wave} = \frac{Area}{\int_0^{1.5} \sin\left(\frac{2\pi}{3}t\right) dt}$$

In this equation “Area” corresponds to the cross-sectional area of the displaced water, while the integral represents the wave. Dividing the area of the displaced water by the wave, the height of the wave can be obtained. Since one wave should occur every three seconds in order to model real ocean waves, the wave will reach its maximum height at 1.5 seconds.

Unfortunately, this equation proves to be inaccurate due to velocity differences between the board and the water. As the board moves forward, the water travels away from the board at a faster velocity, meaning that some of the water volume is lost in the process. To achieve the most accurate measurement, iterative calculations were performed in a variable experiment study to determine when the board velocity approached the wave velocity. For the variable experiment study, the board height, diameter of the cam, initial angle of the board, and height of the water were all considered. By changing these input parameters, the board velocity, wave velocity, and area of displaced water were determined for each scenario. A diagram relating the water height, board height, initial and final board angles can be seen below.

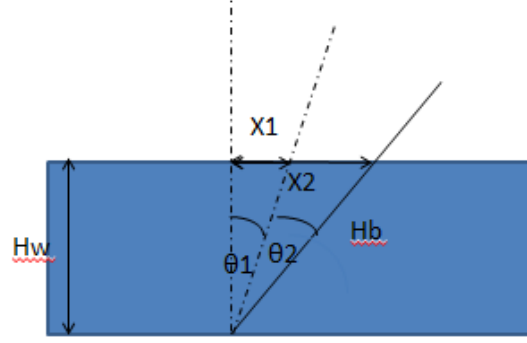


Figure 10: Diagram for Wave Height Determination

In this visual representation h_w , h_b , θ_1 , θ_2 , x_1 , x_2 represent the height of the water, height of the board, initial angle of the board, final angle of the board, initial x direction distance, and final x direction distance, respectively. Of these values, the height of the water, height of the board, and initial angle are all input variables. θ_2 is a calculated value that comes directly from the cam diameter (d) and board height. Since h_b , h_w , cam diameter (d), and θ_1 are all dependent variables, θ_2 can be calculated by:

$$a^2 = b^2 + c^2 - 2bc * \cos A$$

$$d^2 = h_b^2 + h_b^2 - 2h_b^2 * \cos(\theta_2)$$

$$\cos(\theta_2) = \frac{(2h_b^2 - d^2)}{2h_b^2}$$

$$(\theta_2) = \cos^{-1} \frac{(2h_b^2 - d^2)}{2h_b^2}$$

Additionally, x_1 and x_2 can be determined by:

$$x_1 = h_w \tan(\theta_1)$$

$$x_2 = h_w \tan(\theta_2)$$

Knowing, x_1 , x_2 , h_w , θ_1 , and θ_2 , the area of the displaced water can be calculated:

$$Area = \frac{1}{2} * h_w^2 (\tan(\theta_1 + \theta_2) - \tan(\theta_1))$$

Additional parameters that were established through this study included the board velocity and wave velocity. Board velocity was determined by dividing the throw distance, which is the entire distance the board travels in the positive x direction, by half of the time period (1.5 seconds).

Wave velocity was calculated by using the formula:

$$v_{wave} = \sqrt{\frac{2g(\text{throw distance})}{2\pi}}$$

Varying one input at a time while keeping the others constant allowed for finding the specifications that resulted in the smallest difference in wave versus board velocity. This analysis showed that in order to keep the velocity difference small, a larger board height, smaller cam diameter, lower initial board angle, and lower water height were essential. Although a lower water height kept the velocity difference small, a water height of at least 12 inches was needed in order to neglect frictional forces from the bottom of the tank. Ultimately, a board height of 24 inches, cam diameter of 2 inches, initial board angle of 0 degrees, and a water height of 12 inches was found to give the smallest difference in velocities. Although the velocity difference was minimal, the board and wave velocity were not equal, meaning that some of the displaced water volume was lost in the process. To account for this loss in volume, an assumption was made that 25% of the displaced water would be transmitted to the wave volume. This assumption was made based off of a velocity difference of approximately 10.4 inches/sec. From this assumption, it was calculated that the wave height would be approximately 2.5 inches.

3.3.2. Geometry of Four Bar Mechanism

After some of the parameters were set to achieve the desired wave height, the appropriate geometry of the four bar mechanism was developed. Measurements needed to be specified, such as where the crank should be placed relative to the rocker and how long the connecting rod should extend. These geometric specifications were resolved using data from the variable experiment study as well as Linkages software by Norton.

In order to establish the appropriate geometry it was essential to understand the necessary constraints. From the wave height calculations, the board height, cam diameter, water height, and initial start angle must be 24 inches, 2 inches, 12 inches, and 0 degrees, respectively. From these input parameters, it was also found that the board would rotate approximately 5 degrees (θ_2) in order to achieve the desired wave height. Using these dimensions, a model of the four bar linkage was developed in Linkages.

Iterative attempts were completed to find which rod lengths and crank versus rocker dimensions resulted in the correct initial and final board angles. To complete this analysis, the board and cam lengths remained constant, while the x and y distances of the rocker in comparison to the crank were adjusted. As those distances were changed, the rod length needed

to be adjusted accordingly. It was essential to begin the board at a 90-degree angle with respect to the bottom of the tank and finish its forward movement at an angle of approximately 85 degrees. After several attempts were completed, results showed that the rod must be 19.5 inches, and the center of the cam and bottom of the board must be located 18 inches apart in the x direction and 28 inches apart in the y direction to achieve an approximate 5 degree pivot angle with a board of 24 inches. A sketch with these measurements can be seen below:

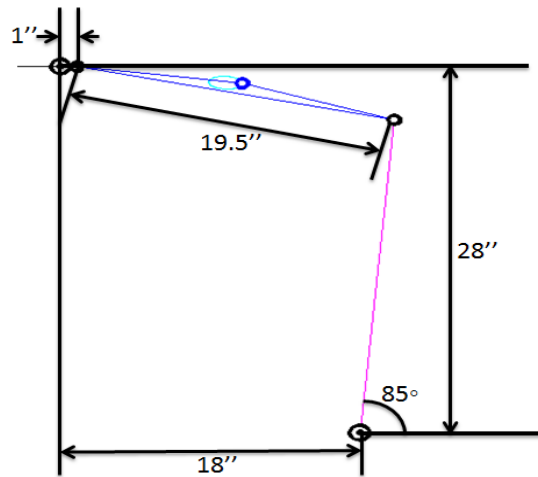


Figure 11: Wave Generator Geometry

Using this software, the wave generation mechanism was set up according to this geometry.

3.3.3. Power Requirements & Motor Preparation

In addition to the proper geometry for setup and the estimated wave heights, the power requirements for the system also needed to be calculated. To generate the required waves, a motor that could push the water at the desired speed was needed. Power can be calculated by multiplying torque by angular velocity. The angular velocity was previously found to be 20 RPM based off the knowledge that one wave should occur every three seconds; therefore, torque acting on the motor was the only variable that needed to be defined. To find this value, the kinematics of the wave generation system were analyzed by starting with the forces exerted on the board and then continuing upwards through the entire wave generating mechanism.

The board was the first piece to be evaluated because of its direct interaction with the water. Looking at a free-body diagram of the board (Figure 12), the forces that act on it include the force of the rod in the x direction as well as the force of the water and weight of the board.

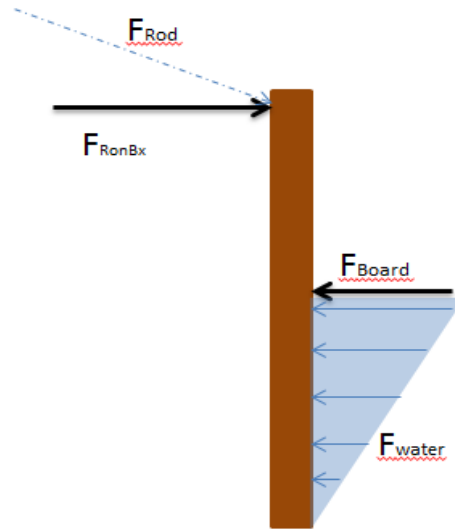


Figure 12: FBD of Board

The force of the rod in the x direction was determined by understanding that the rod creates torque equal and opposite the board and water about the hinge. To define the torque, and thereby the force that the rod exerted, calculations for the torque from the board weight and water were completed. The torque of the board was calculated by the following steps in which “r” is half the length of the board (12 inches), “ θ ” is the angle that the board rotates (5 degrees), “t” is half of the time interval (1.5 seconds), and “ m_b ” is the mass of the board (4 kg). From these calculations it can be seen that the torque from the board is approximately 0.014J.

Torque from Board

$$vel_{ib} = 0 \frac{in}{s}$$

$$vel_{fb} = \frac{r\theta}{t} = 0.67 \frac{in}{s}$$

$$a_b = \frac{(vel_{fb} - vel_{ib})}{t} = 0.45 \frac{in}{s^2}$$

$$F_b = m_b a_b = 0.045 N$$

$$\tau_b = F_b r = 0.014 J$$

Calculating the torque from the water was more complex for multiple reasons; there was water on both sides of the board and the torque of the water varies with different distances from the hinge. To account for the water being on both sides of the board, the force of the water was doubled, and to account for the varying torque, an integral was computed over the varying water

heights (0-12 in). The mass of the water was determined by multiplying the density times the volume of water that was displaced. The steps for those calculations can be seen below. In the calculations ρ , dA_b , h , Θ , t , and w_{tank} , represent water density, changing cross-sectional area, water height, board angle, time elapsed, and width of the tank, respectively.

Torque from Water

$$dF = 2 * \rho * A_b * \frac{h^2 * \theta^2}{t^2}$$

$$\tau_{H_2O} = \int_0^{12} h dF$$

$$\tau_{H_2O} = \int_{0in}^{12in} \left(2\rho \frac{h^3 \theta^2}{t^2} w_{\text{tank}} \right) dh = 0.012 J$$

Knowing the torque of the water and board was equal and opposite the torque of the rod, the force that the rod exerts in the x direction was calculated by adding together the torque from the water and board and then dividing by the distance of the rod to the hinge (24 inches). From that calculation, the rod exerts a force of 0.043N in the x direction, as can be seen below.

$$F_{\text{RonBx}} = \frac{\tau_b + \tau_{H_2O}}{24 \text{ in}} = 0.043N$$

The next step was to find the force that the rod exerts on the cam. Since the rod is pinned at both ends and carries no other loads, it was simplified into a two-force member. The two forces acting on the rod were the force of the board and the force of the cam. When modeling a two-force member, the forces are equal and opposite when they act along the centerline of the member. Knowing the force that the rod exerts on the board in the x direction, the force that the board exerts through the centerline of the rod was calculated by finding the angle that the rod makes in relationship to the horizontal. A free body diagram of the rod is shown in Figure 13.

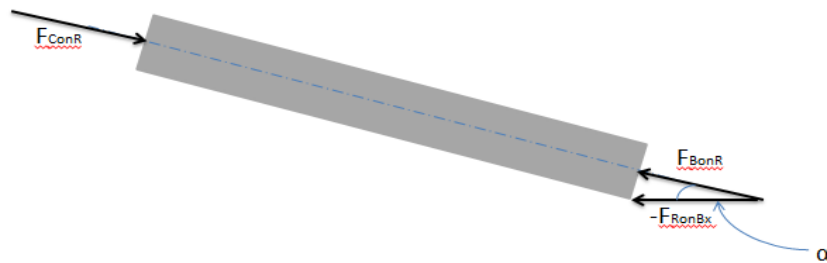


Figure 13: FBD of Rod

The angle of the rod was computed using the length of the rod, as well as the angle of the cam when the board was upright. The length of the rod was 19.5 inches, forming the hypotenuse

of the triangle, while the distance in the x direction was 18 inches plus the extra x direction distance due to the 18-degree angle of the 1 inch cam. From these dimensions, the angle formed by the rod was 14 degrees. Knowing the angle that the rod forms, the force exerted on the rod along its centerline was resolved.

Forces on the Two Force Member (Rod)

$$L_{rod} = 19.5 \text{ in}$$

$$d_x = 18 \text{ in} + \cos(18) * 1 \text{ in} = 19 \text{ in}$$

$$\alpha = \text{acos}\left(\frac{d_x}{L_{rod}}\right) = 14 \text{ deg}$$

$$F_{BonR} = \frac{F_{BonRx}}{\cos(\alpha)} = -0.044N$$

$$F_{ConR} = F_{BonR} = 0.044N$$

This concluded that the force of the cam along the centerline of the rod was 0.044N.

By analyzing the cam further, the force that it exerts perpendicular to its moment arm was calculated. A free body diagram of the cam is seen in Figure 14.

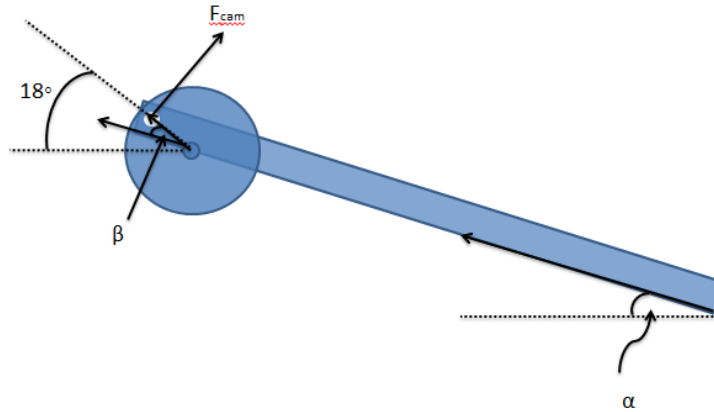


Figure 14: FBD of Cam

By setting the angle, β, and then multiplying sin (β) by the force of the cam along the centerline of the rod, the force of the cam was determined. These calculations are seen below.

$$\beta = 18 - \alpha = 4.4 \text{ deg}$$

$$F_{cam} = \sin(\beta) * F_{ConR} = 3.2 \times 10^{-3} N$$

Multiplying this force by its moment arm resulted in the torque produced by the cam. Since the moment arm in this case is the radius of the cam (1 inch), the torque was found to be $8.0 \times 10^{-5} \text{ J}$.

In order to find the power required from the motor, the torque of the cam was multiplied by the angular velocity of the motor to give a power requirement of $1.7 \times 10^{-4} \text{ W}$. This means that

in order to produce 2.5 inch waves in the small scale system about 0.17 mW of power was required.

After completing calculations for the power requirements, the next step was finding an acceptable motor for this system. A 226 Series Gearhead Motor from AM Equipment was acquired and found to produce as much as 71 W of mechanical power, enough for the wave generation system. The specification sheet for this particular motor can be found in Appendix A. Although this motor was capable of producing the required power, the torque exerted on the shaft from the water and board was not significantly high, which caused the motor to operate too fast. In order to alleviate this problem, a pulse width modulator was created in order to slow down the speed of the motor.

To slow the motor to 20 RPM to account for wave scaling factors and a wave frequency of 20 waves per minute, different options were explored. While gears or other mechanical devices were considered, it was decided to minimize power losses and as such use an electronic circuit. The specific circuit chosen falls in the category of a Pulse Width Modulator (PWM). The function of a PWM is to essentially act as a controllable timed on and off switch with a high frequency that turns a constant DC Voltage (such as that delivered from a car battery) into something resembling a Square Wave. Ideally a PWM can control both the frequency of the output function as well as the duty cycle, which is defined as the ratio of on and off time, or the width of the square wave. Figure 15 illustrates the variety of output functions that a PWM can produce as well as a variety of functions with differing duty cycles. The percentage values are equivalent to the duty cycle of each wave.

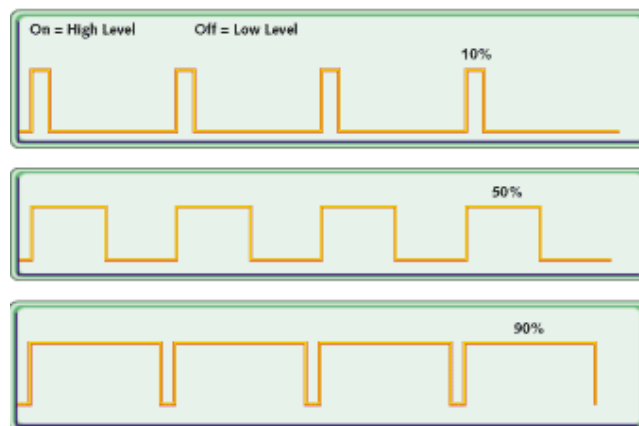


Figure 15: Variety of Duty Cycle Outputs Generated by PWM

The PWM design had to be highly controllable to account for different testing parameters, while also minimizing power losses and maximizing power output. The circuit design that was employed is pictured in Figure 16. This specific circuit uses a NE555N timer as its centerpiece, two potentiometer (variable resistors) to control both the frequency and the duty cycle of the output function, two MOSFET IRF 520 switches to aid in heat dissipation and a number of protective diodes and capacitors.

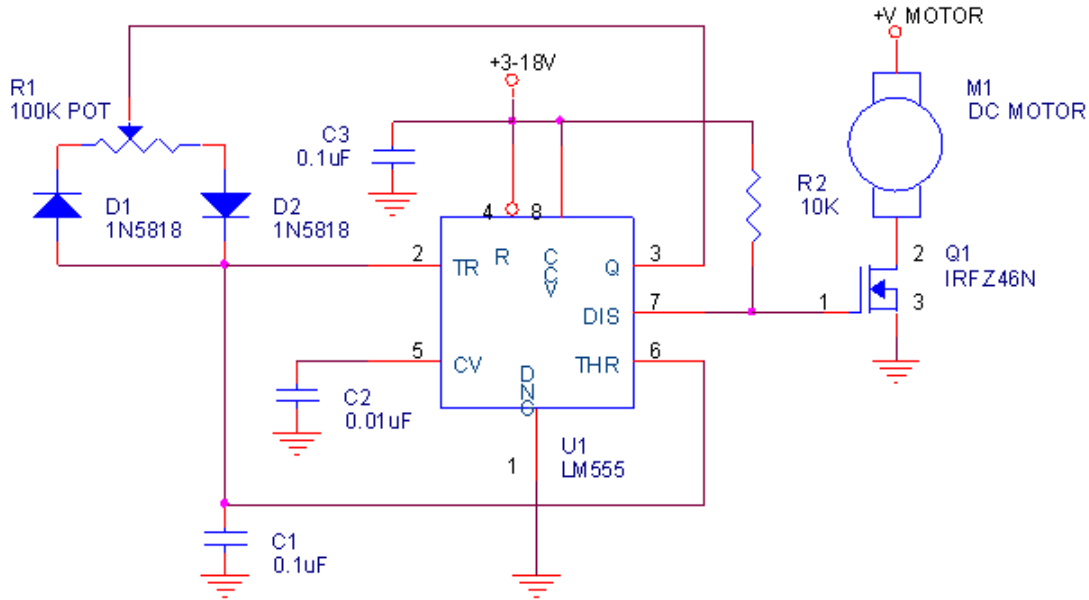


Figure 16: Circuit Diagram of Pulse Width Modulator

After the PWM was created, the motor was prepared to be used in the wave generation system. Preparation included machining a press fit linkage to the motor's shaft. After measuring the shaft dimensions, interference calculations were completed by finding the pressure and torque of the shaft within the hub of the linkage. Using an interference of 0.001 inches, pressure was calculated by:

$$P = \frac{0.5\delta}{\frac{r_h}{E_o} * \left(\frac{r_o^2 + r_h^2}{r_o^2 - r_h^2} + v_o \right) + \frac{r_s}{E_i} (1 - v_i)}$$

Where r_s , r_h , r_o , δ , v_o , v_i , E_o , E_i , represent the shaft radius, inner hub radius, outer hub radius, difference between shaft radius and inner hub diameter, Poisson's ratio of the hub material (6061 Al), Poisson's ratio of the shaft material (steel), the elastic modulus of the hub, and the elastic modulus of the shaft, respectively. The torque was calculated by:

$$T = 2\pi r_s^2 \mu Pl$$

μ represents the coefficient of friction between the shaft and hub and l represents the length of contact between the two interfaces. From the pressure and torque calculations, an interference of 0.001 inches was sufficient to create a proper press fit. A model of the linkage, seen in Figure 17 below, was designed while taking the necessary interference into account.

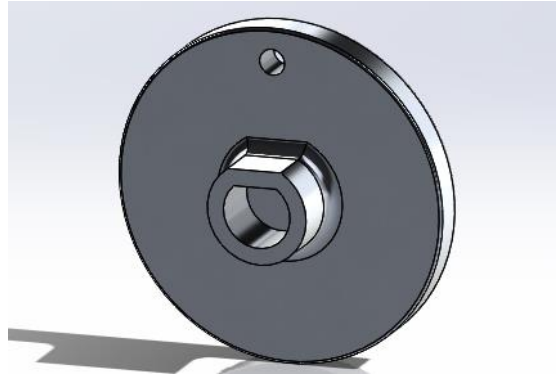


Figure 17: Motor Cam

Once the model was designed, it was then manufactured using 6061 aluminum at the machine shops in Washburn. The stock metal was first shaved down to the proper dimensions in the lathe and then the mill was used to perform the drilling operations. The linkage was then press fit to the motor shaft by heating up the metal and then applying force. Once cooled, the linkage was securely fastened to the motor shaft as seen in **Error! Reference source not found.**, which completed the motor preparation.



Figure 18: Cam Attached to Motor

3.3.4. Stresses Exerted at the Joints

Along with finding the power requirements of the system, another important factor to consider was the stress exerted at various joints. In the wave generation system there are four major areas of stress concentration; the two hinges connecting the board to the test tank, the pin connecting the rod to the board, and the pin connecting the rod to the cam. Each of these stress concentrators was analyzed to ensure that they would be capable of handling the necessary loading conditions. The first area that was dissected included the hinges connecting the board to the bottom of the tank. A schematic with the loading conditions can be seen below:

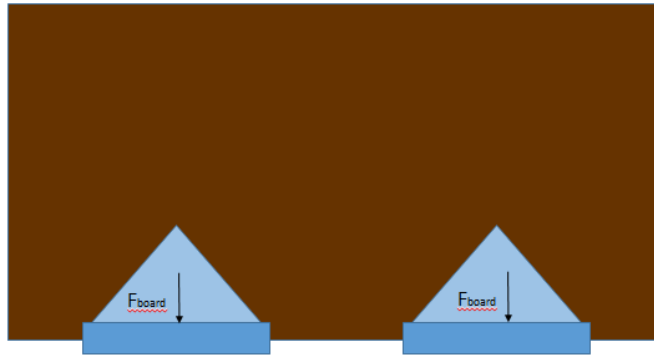


Figure 19: Hinges Connecting Board to Test Tank

The only force that is exerted on the hinges is the force of the board. Since the hinges have a 0.5 inch diameter and the force of the board can be split amongst the two hinges (assuming that the hinges are positioned symmetrically about the board), the shear stress exerted on each hinge can be calculated by:

Shear Stress on Hinges Connecting Board to Test Tank

$$D_{hinge} = 0.5 \text{ in}$$

$$Area_{hinge} = \pi \left(\frac{D_{hinge}}{2} \right)^2 = 1.3 \times 10^{-4} m^2$$

$$\tau_{hinge} = \frac{m_b * g}{2 * Area_{hinge}} = 1.5 \times 10^5 Pa$$

Each hinge experiences a shear stress of 0.15 MPa. This means that they will be more than capable of handling the stress exerted on them since they are made from steel, which has a shear strength ranging from 165-1130 MPa.

The next joint that was taken into consideration included the pin connecting the rod to the board. The forces exerted on this pin included the force of the board as well as the force of the rod. Figure 20 shows a free body diagram of this pin joint.

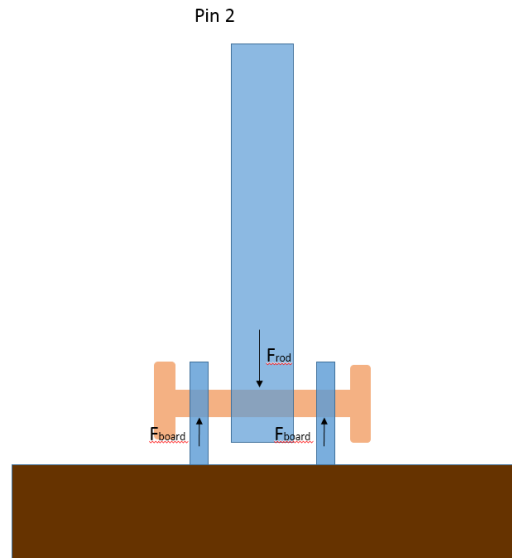


Figure 20: Pin Connecting Rod to Board

Since the board is connected in two different locations, the pin experiences double shear, meaning that the stress is cut in half. Calculations for the shear stress exerted on this pin can be seen below:

Shear Stress on Pin Connecting Board and Rod

$$D_{pin2} = 0.5 \text{ in}$$

$$Area_{pin2} = \pi \left(\frac{D_{pin2}}{2} \right)^2 = 1.3 \times 10^{-4} m^2$$

$$\tau_{pin2} = \frac{-F_{BonR}}{2 * Area_{pin2}} = 163 \text{ Pa}$$

The shear stress at pin 2 is only 163 Pa. Since pin 2 is also made from steel, there is no concern about the pin experiencing failure in this environment.

The final joint that was analyzed was the pin connecting the cam to the rod. As seen in Figure 21, the forces that act on this pin include the force of the cam and the force of the rod, which were previously determined to be equal and opposite.

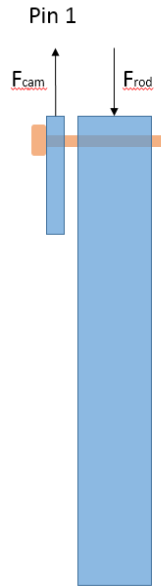


Figure 21: Pin Connecting Cam to Rod

To determine the shear stress acting on pin 1, the force exerted on the pin was divided by the cross-sectional area of the pin. The pin used in the system is approximately 0.190 inches in diameter. The calculations for the shear stress can be seen below:

Shear Stress on Pin Connecting Cam and Rod

$$D_{pin1} = 0.190 \text{ in}$$

$$Area_{pin1} = \pi \left(\frac{D_{pin1}}{2} \right)^2 = 1.8 \times 10^{-5} m^2$$

$$\tau_{pin1} = \frac{F_{ConR}}{Area_{pin1}} = 2.3 \times 10^3 Pa$$

The shear stress acting on pin 1 is 2.3 kPa. Since this pin is also made out of steel, it will be able to handle the testing environment. This shows how all areas of stress concentration will remain intact.

3.3.5. Other Considerations

Other important components of the wave generation system included its overall features. The system was placed in a large wooden test tank. The test tank was 8 feet long, 3 feet wide, and 2 feet deep. In order to keep the tank waterproof, it was coated with a water resistant layer and then sprayed with a rubber sealant along all the edges. Additionally, the tank was made with no legs so there would be no concentrated areas of stress. Wooden supports were placed underneath and along the edges of the tank for extra stability and security.

It was essential to ensure that the electrical components did not interact with the water. To do this, the motor was mounted four inches above the top of the test tank by means of a slotted L-bar. A U-clamp tightly secured the motor to the L-bar. Additionally, a 12-volt car battery was placed on the ground behind the motor. The battery was covered and shielded by a plastic tarp. The pulse width modulator was placed on a flat surface next to test tank, ensuring that it would not fall into the filled tank. The necessary precautions were taken in order to keep the team safe as well as keep the equipment from being damaged.

3.4 Design of Overtopping Device

By combining the desirable aspects of Wave Dragon and SSG as discussed in Chapter 2, a new overtopping device was designed as shown below in Figure 22. The device consists of three tiers of reservoirs that empty into each other. In the actual device a multi-stage turbine would connect each tier, converting the stored potential energy into power, however, due to the small-scale nature of this prototype, the turbine was omitted. The device was attached to the test tank to mimic anchoring and avoid movement during wave simulations and testing. The device was designed to continuously operate, as waves will constantly be entering at least one of these three tiers due to the slight bottleneck design. Consistent operation allowed the overtopping device to reach higher efficiencies than other systems.

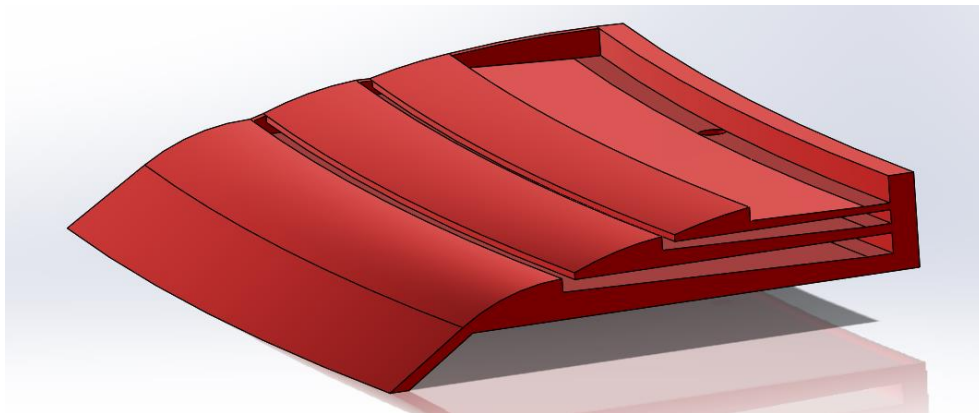


Figure 22: Overtopping Prototype

An actual full-scale design would incorporate wave reflectors on each side in order to maximize the amount of waves that are captured. For the purpose of this project, the wave reflectors were omitted due to size limitations of the test tank.

This particular prototype can be broken into three main design categories that are crucial to its functionality: tier design, ramp design, and tier drain system.

The prototype was designed so that the tiers optimally function under 2.5 inch waves. As mentioned previously in chapter 3.2.: tier one has a relative height of 0.6 times the wave height, tier two has a relative height of 1.0 times the wave height, and tier three has a relative height of 1.2 times the wave height. Each tier is tapered so that the water is forced to flow towards the back of the device where it is outputted to the draining system. The bottom of the prototype is shelled out so that the device is able to float above the water. Not only does this allow the device to float, but it also allows water flow out of tier 1. Without a pocket of air there would be no potential energy, restricting any volume of water from flowing out of tier 1.

Another important part of the device design is the ramp. A wave is felt up to half its wavelength under water, therefore the bottom ramp, leading to tier 1, is designed to account for the felt wave height. Since the wave will break on the prototype, there will not be any disturbances under the device. The ramps leading to the higher tiers are overlapped such that if the wave does not make it all the way up the ramp, it will fall back down into the previous tier. This is shown in the image below:

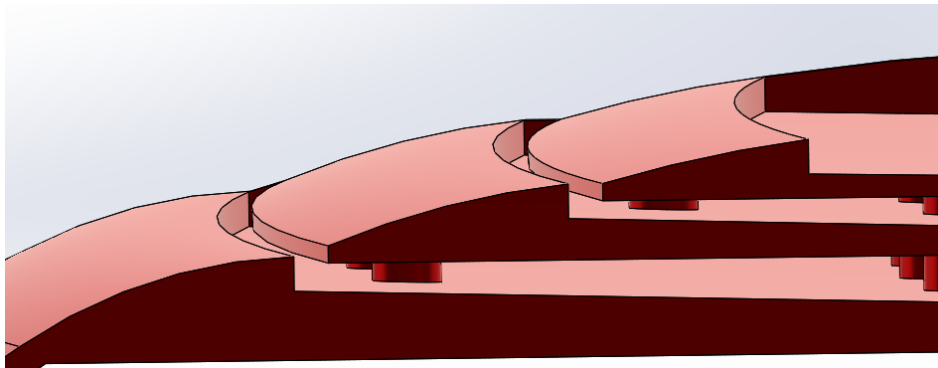


Figure 23: Ramp Design

Producing a turbine for this prototype was not possible due to budget and size constraints, so to simulate the actual output of a turbine, the theoretical power output was calculated by measuring the volume of water that was captured. A hole was drilled through all 3 tiers of the device to drain water entering the system. The tiers were designed to fill at the same rate as they were draining in order to maintain a constant head. By maintaining constant head, the prototype can fulfill both the minimum head requirement and constant operation for the turbines.

A piping system was developed, enabling water to be captured from one tier while closing off the other two. To do this, a pipe fitting was inserted in the hole that extends through all three tiers. At each tier level, a hole was cut in the pipe fitting allowing water to flow out of

all tiers simultaneously. A smaller pipe that fit tightly inside of the pipe fitting was broken into six evenly spaced sections. As shown in Figure 24. Each odd numbered section was designed to drain one tier specifically. For example, when Section 1 is aligned with the holes of the outer fitting, tier 3 is able to drain while the other two remain shut. Section 3 and 5 enable tier 2 and tier 1 to drain, respectively. Each even numbered section is designed to block off all tiers.

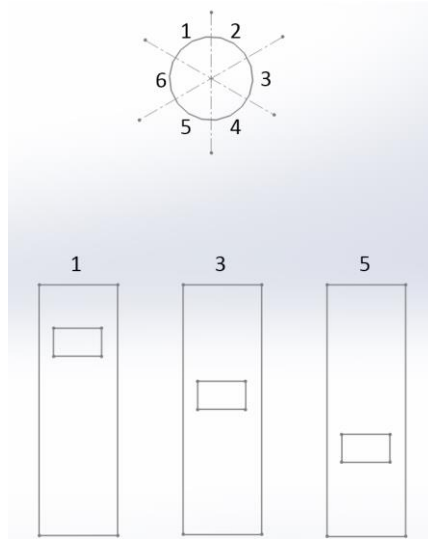


Figure 24: Tier Section Design

These sections have two purposes: one is to stop draining a tier successfully without opening the hole of another tier and the second is so the optimization of maximum head is possible before opening the channel of a tier to drain. Figure 25 below shows section one of the tier drain system.



Figure 25: Tier Drain System

3.5 Construction of Test Tank and Device

3.5.1. Test Tank Construction

The wave tank was constructed to test the wave energy converter while simulating deep-water waves. The wave tank was constructed from 2x6's and $\frac{3}{4}$ " plywood. The tank is illustrated in the SolidWorks drawing and model below.

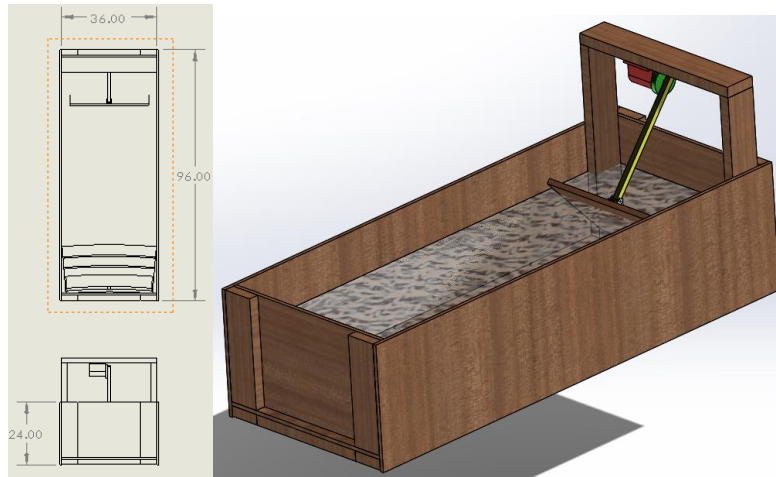


Figure 26: SolidWorks Drawing and Model of Wave Tank

Construction began by cutting all pieces to the proper dimensions: two 8'x2' side pieces, two 3'x2' pieces for the front and back, and one 3'x8' bottom piece. Once all pieces were cut, the frame was built by attaching the 2x6's with supporting joints at the corners for added strength. The plywood was then added to this frame for enclosure of the tank. Additionally, supports were added at the center of the tank to prevent collapsing under a heavy load of water. In order to ensure the waterproof interior, latex was coated along the inside with rubber spray lining the seams of the tank. The exploded view below illustrates the assembly process of the wave tank.



Figure 27: Exploded View and Final Construction of the Wave Tank

3.5.2. Device Construction

In order to utilize the resources available for manufacturing, each tier was broken into 3.5" wide segments that could be easily machined. To achieve the desired slope across the entire device, a continuous slope was cut across each segment to form a continuously flowing piece. The sloped tiers were created by machining grooves in a small metal block at the correct slope and resting each board on the block to be machined. Due to the 3' length of the board, the milling tool experienced a great deal of chatter during the cutting operation. To ensure a smooth surface finish, a metal rod was taped to the underside of the board to add mass and minimize chatter. This same process was utilized to create all three tiers of the device.

Once all of the slopes were machined, the tiers required assembly of the 3.5" wide segments using a technique called biscuit jointing. Biscuit jointing involves a process of cutting small slots in the material and inserting wooden biscuits that hold the pieces together.

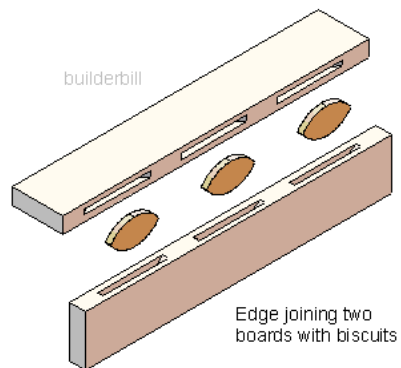


Figure 28: Biscuit Joint Exploded View (Biscuit, n.d.)

Biscuit jointing was used on each of the three tiers consisting of five, four, and three segments for tiers one, two, and three respectively. The tiers were glued with PVC cement and clamped together to allow for proper setting and drying of the tiers.



Figure 29: Clamped Tier 1 to Allow Proper Setting Of Biscuit Joints

Following the assembly of the tiers, the sideboards and backboards were constructed to support the system. The cuts were easily achieved by creating dxf files exported to the CNC mills, which quickly cut the tier cross-section into the sideboards.



Figure 30: Cross-Section of the Sideboards

The tier slots were cut 0.375” deep into the PVC trim to provide as much support as possible for each reservoir without compromising the integrity of the sideboards. The two sideboards were created as mirror images so as to hold the tiers in their respective slots.

Finally, the backboard was created to close off each reservoir and provide extra structural support for each tier. The backboard was created in a similar fashion to the sideboards, using CNC milling which was established by the SolidWorks image illustrated below.

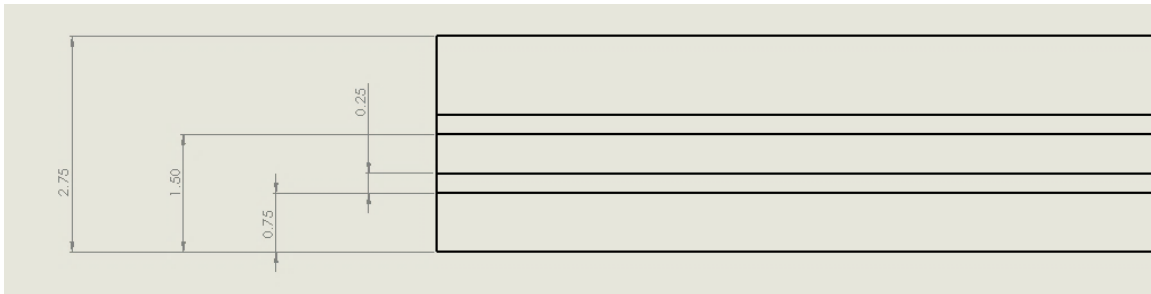


Figure 31: SolidWorks Drawing of the Backboard

The simplistic design for the backboard allows the back to sit on the bottom tier to maximize support from this level and provides slots for the remaining top two tiers cut at the same depth as the sideboards at 0.375”. Concluding the machining of the tiers, sideboards, and backboard, the pieces were all assembled using PVC cement and clamped in place for proper setting.

3.5.3. Assembly of Testing Unit

Upon completion of machining the wave energy converter, additional assembly was required to account for the testing procedure. To provide a means of capturing and measuring volume, an expansion adapter tube was inserted into the device. A hole of diameter 2.81” was machined in the back center of each tier to produce a continuous hole throughout the device. To

accommodate the flow of water through each tier, CNC milling was used to create openings for each level of the expansion adapter as shown below.

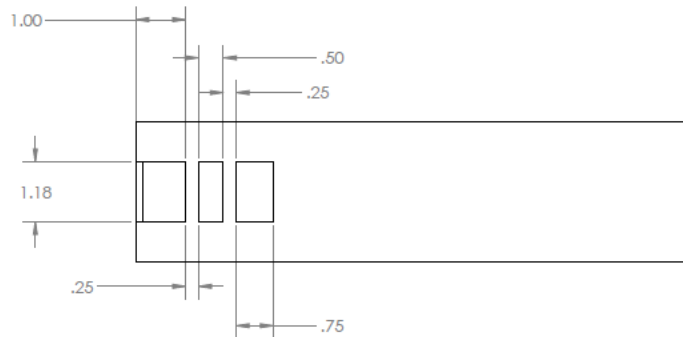


Figure 32: Drawing of Expansion Adapter for Water Collection

Each opening lines up with the three tiers and provides a tight seal using PVC cement to waterproof and lock the expansion adapter in place. Furthermore, the inner tube of the expansion adapter was altered to close off flow to all but a single tier at a time. In doing so, the volume can be measured from each tier to determine efficiency of the multiple levels. By removing the inner tube altogether, the entire device can be tested at once in terms of flow and volume capture. The design of the inner tube relies on sealing off two tiers at any given time and therefore, the openings occur at 120° apart from one another as is demonstrated below.

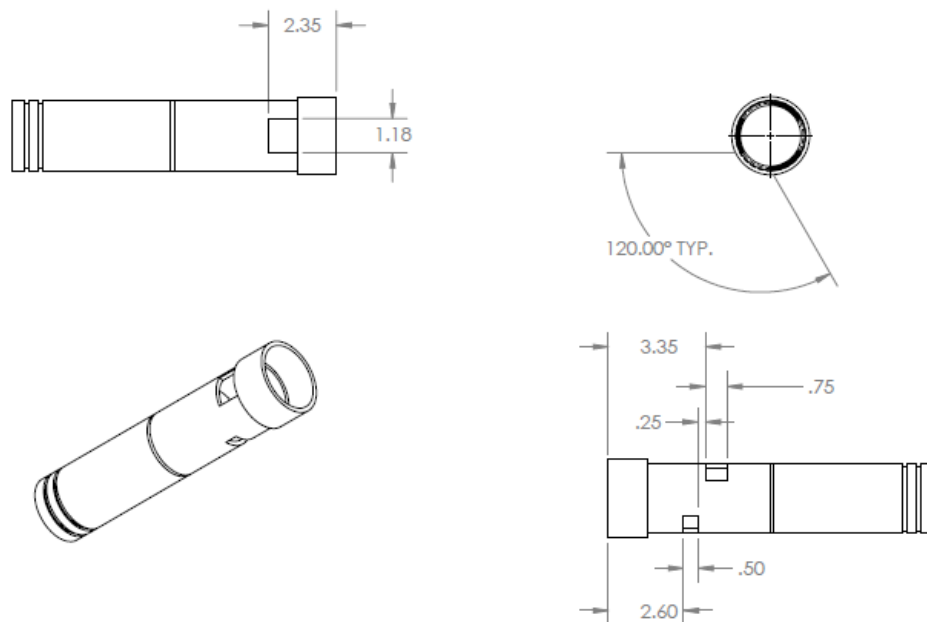


Figure 33: Inner Tube Design for Testing Different Tiers

To achieve proper sealing for each tier, O-ring grooves were cut directly below each opening using a CNC lathe. Therefore, the finished inner tube design functions with offset openings to allow flow through one tier at a time while the watertight O-rings seal each tier.

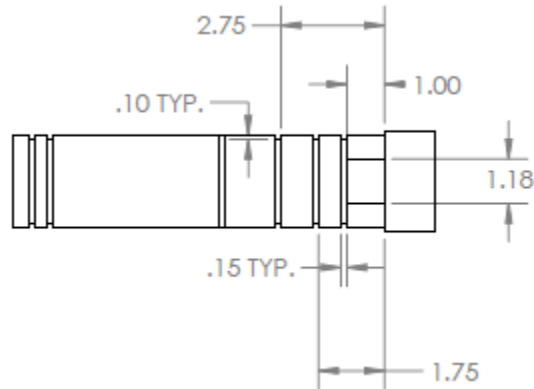


Figure 34: Finalized Inner Tube Design with O-Rings

The final construction steps required the implementation of the wave energy converter into the wave tank. To accomplish this, a reduction hose was implemented to decrease the diameter of the expansion adapter for proper fitting of a hose. This reduction hose was then PVC cemented to a small adapter, providing an outlet for a 2 inch OD tube. An elbow fitting was installed to slope the tube out of the bottom of the device and through a hole in the side of a tank. Large amounts of expansive rubber adhesive and caulk were applied to the boundary of the tube to prevent leaking. Lastly, supporting boards were attached at a height of 12 inches where the bottom of the device will rest during testing. The support boards act as a stabilizing measure to prevent extensive motion of the device while testing is taking place. The final assembly of the device within the tank is illustrated in Figure 35 and Figure 36.

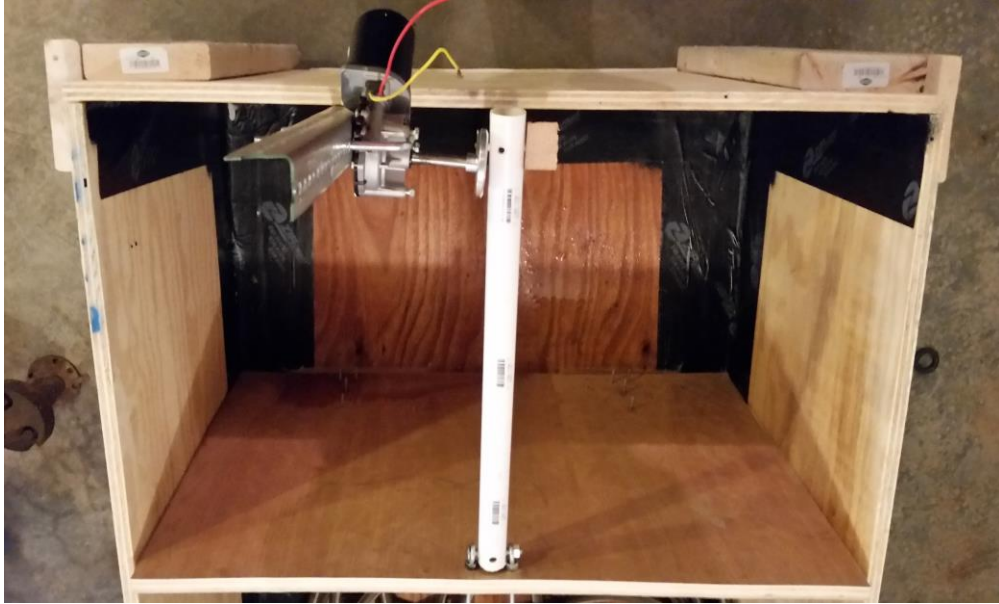


Figure 35: Final Assembly Wave Generator



Figure 36: Final Assembly Wave Converter

Chapter 4 – Testing & Data Collection

Testing of the wave capture device required various data collection to accurately calculate the power output because turbines and generators were not used in the prototype. For this reason, it was important to measure the volume of water captured per wave for each tier as well as the drain time. Additional observations proved the ability of the device to maintain constant head, retain the collected water, and successfully produce flow that would act to spin turbines in a real world model. Tests were completed to define the success of scaling up the prototype to be used in marketable applications.

The first test for the wave capture device was to measure the amount of volume captured per wave during operation. Results were achieved through a series of steps. First, the tank was run without collecting any water until the waves reached a steady state condition. The characteristic waves needed to be attained before collection to perform repeatable tests. The characteristic wave created during the test can be illustrated in Figure 37.

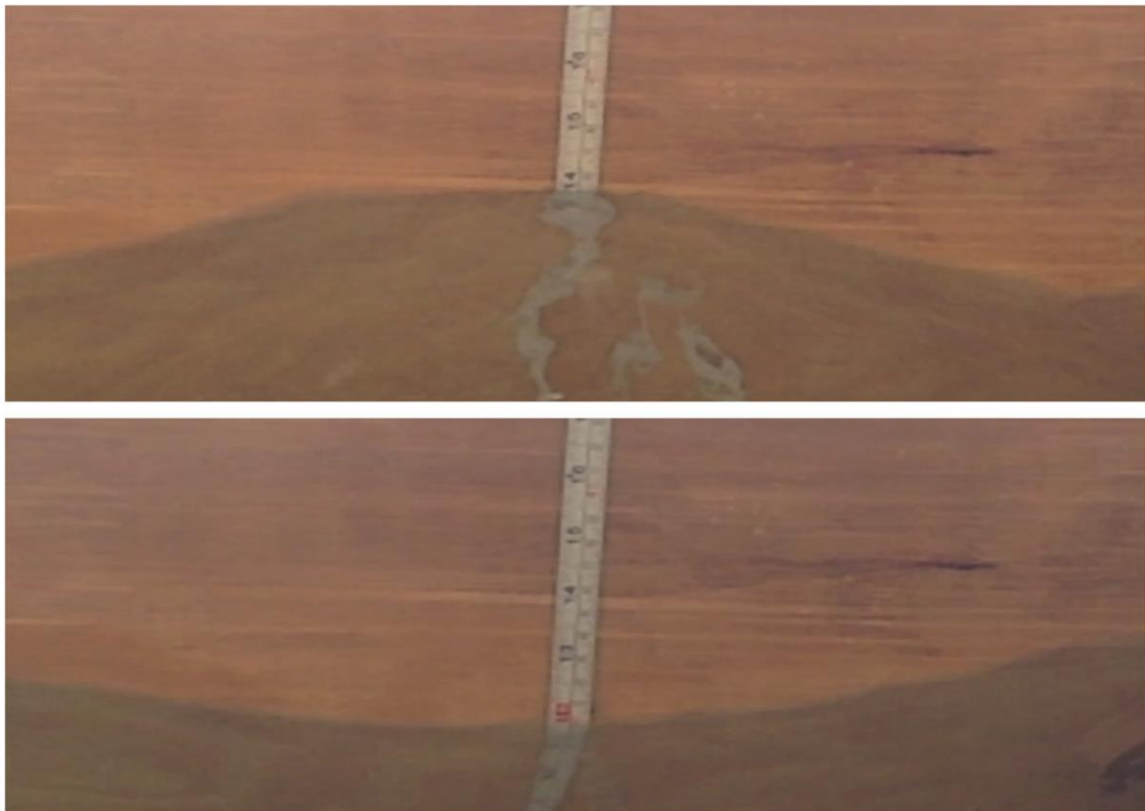


Figure 37: Characteristic Waves

As can be seen in Figure 37, the wave amplitude was about 2.5 inches. As explained in the previous calculations, the actual wave height is equal to half of the amplitude. Therefore, the waves were about half of the desired height of 2.5 inches at about 1.25 inches for testing. .

The next step was for the device to collect water for a series of 60 waves. The number of waves was counted once more to maintain a repeatable test that would theoretically sustain equal volumes of water collected for each trial. The water drained from the device through a piping system into a container for water collection. The container was weighed both before and after collection using an eye-level beam scale to determine the mass of water collected. Using the mass and density of collected water, the volume could then be calculated knowing that:

$$V = \frac{m}{\rho}$$

Initially, all tiers were left open and the entire volume collected from the device was measured. Afterwards, different tiers were blocked off to analyze the contribution from each tier individually. To do so, an inner tube was used in the wave capture device to block off all but one tier during testing. First, the top two tiers were blocked off and the bottom tier was tested for water collection. Next, the top and bottom tiers were blocked off and the middle tier was tested for volume capture. Seeing as the water was unsuccessful at reaching the top tier, testing for this tier was omitted. Two trials were completed to ensure repeatability and accuracy, which proved to be consistent between tests. The table below displays the results yielded from each of the tests.

Table 3: Volume Collection Data

Trial #	Bucket Weight (lb)	All Levels (lb)	Volume (GPM)	2nd Tier (lb)	Volume (GPM)	Bottom Tier (lb)	Volume (GPM)
Trial 1	1	29	209	6	43	26	187
Trial 2	1	28	201	5	36	22	158
Avg. Weight		28.5	53	5.5	10	24	45
Avg. Weight without bucket		27.5	198	4.5	32	23	165

Further tests were completed to determine the flowrate of the collected water out of each tier. The test was performed by blocking off a single tier and filling it with water. Once the tier was full, the inner tube was removed to drain the tier. The tier draining time was measured to

calculate the flowrate of water out of the device. Two trials were completed to demonstrate repeatable results. The recorded times and calculated flowrates are shown in the table below.

Table 4: Drain Time and Volumetric Flowrate

Emptying Time	Bottom Tier (s)	Volumetric Flowrate (GPM)	Middle Tier (s)	Volumetric Flowrate (GPM)
Trial 1	86	1.16	73	0.67
Trial 2	78	1.28	70	0.70
Average	82	1.22	71.5	0.69

Further observation of the device during testing revealed that the device did not leak. Additionally, the device successfully maintained constant head throughout each test. The data compiled from this testing was interpreted into power outputs that could be yielded from a life-size model.

Chapter 5 – Results & Analysis

Testing of the wave energy converter device returned promising results. A fundamental outcome achieved was the ability of the device to maintain constant head throughout testing. This means that the device was able to sustain a steady water level in the reservoirs of both the bottom and middle tiers even as water drained from the device and was collected. The lack of constant head in many current systems prevents the turbines from consistently operating. The purpose of constructing a device that is capable of keeping a constant head is to reduce inefficiencies. The energy required to overcome static friction to begin turning a turbine is higher than that required to retain motion of an already spinning blade. With a constant water level, the turbines will not stop as long as waves are being generated. This will minimize the frictional losses due to the starting and stopping of the turbine. On the other hand, if the tier is draining slower than it is filling, it will become saturated and the volume capture efficiency will decrease. Therefore, it is important to optimize the number of turbines in the system to drain the device at the same rate that it is being filled.

Further analysis demonstrates the success of the design to capture and hold a large volume of water without creating high stress concentrations causing any damage to the device. Observations show the water's ability to travel up the device, collect in each reservoir, and withstand the forces produced by the waves. Although this observation appears trivial, there is a direct correlation between the structural integrity and implementation costs. Although the design was successful in providing a ramp to capture water in the first two tiers, the third tier was unsuccessful in collecting water at all. This suggests that either the waves produced were simply not large enough in regards to the prototype scale or the scaled device dimensions should be shifted to account for this currently extraneous component.

To quantify the success of the system in wave volume captured, the efficiency can be calculated using the theoretical wave volume compared to the actual volume collected. The volume of the wave can be estimated by the integral of a sine curve with a peak at 1.25 inches multiplied by a width of 36 inches. The theoretical volume of the wave is then represented by:

$$V = \int_0^{\pi} 1.25 \sin t \, dt * 36$$
$$V = 36 * 1.25 [(-\cos(\pi)) - (-\cos(0))] = 90 \text{ in}^3$$

The collected volume represents the water captured for a total of 60 waves and therefore the theoretical volume should be extrapolated to 60 waves by:

$$Total\ Theoretical\ Volume = V * 60 = 5,400in^3$$

The actual collected volume can then be obtained from the data in the previous section. Using the average volume of water collected from the three tiers gives a value of $762in^3$.

The efficiency of wave collection can then be calculated comparing the theoretical collection value to the experimental collection value as:

$$Collection\ Efficiency = 1 - \frac{5,400 - 762}{5,400} \times 100\% = 14.1\%$$

Although the collection efficiency seems low, this is the efficiency before optimization of turbines. In the tested system, the first tier filled early in the test and remained saturated for the entirety due to a slower drain rate compared to collection rate. Therefore, the reservoirs were filled and unable to take on any of the extra water. Through optimization of turbines, the collection efficiency approaches 100%, which will be discussed later.

The power output of the system can be determined by using the measured volumetric flow and head, the density of water, the gravity constant, as well as the conversion factors needed to convert the units into watts. Using these parameters, the calculated power output for the prototype can be calculated by:

$$P = \rho qgh * eff$$

Where ρ is the density of water, q is the volumetric flow, g is the gravity constant, h is the head, and eff is the turbine efficiency. The head was measured by the CNC machine used to manufacture the device and the flowrate was calculated based on the mass of water collected from the system. This calculated power output for the prototype scale is illustrated in the table below.

Table 5: Prototype Scale Power Output

Prototype Scale				
Tier	Head (ft)	Volume Flow (GPM)	Calculated Power (W)	Calculated Power (W)/ft of Wavefront
Top	0.021	0.000	0.000	0.000
Middle	0.042	0.686	0.003	0.001
Bottom	0.063	1.221	0.007	0.002
Total			0.010	0.003

The Froude scaling factor was used to scale the prototype to a full-size model of the device. Froude scaling was based on the wave height (λ) for the system and the dimensions of each parameter. For a 1.25 inch wave height, the Froude scaling ratio is defined for the following parameters:

Table 6: Froude Scaling Ratio Calculations

Parameter	Dimension	Froude Definition	Froude Scaling Ratio
Head	[L]	Λ	0.0318
Volumetric Flow	[L ³ T]	$\lambda^{5/2}$	0.00018

Applying these Froude scaling ratios to the prototype scale then yields full-size results as:

Table 7: Full-Size Model Scale Power Output

Tier	Full-Size Model Scale			
	Head(ft)	Volume Flow (GPM)	Calculated Power (W)	Calculated Power (W)/ft of Wavefront
Top	0.7	0.0	0.0	0.0
Middle	1.3	3802.6	469.6	5.0
Bottom	2.0	6769.7	1254.1	13.3
Total			1723.8	18.3

Because the system needs to operate under low head conditions, Kaplan turbines were utilized. These hydro turbines require a minimum head of only 1ft, which best suits this system. The specifications for low-head Kaplan turbine operability are displayed in the table below.

Table 8: Low-Head Kaplan Hydro Turbine Specifications (1000W Low Head Kaplan Turbine, 2015)

Head[Feet]	Flowrate[GPM]	Approximate Production [Watts]	Minimum Pipe Size
1	320	25	8"
2	450	70	8"
3	550	150	10"
4	635	250	10"
5	710	350	10"
6	775	465	12"
7	840	585	12"
8	895	715	12"
9	950	850	12"
10	1000	1000	12"

The specifications of the low-head Kaplan hydro turbine can be used to determine the efficiency of the system. Without considering the turbine efficiency, the power output would be inaccurate since it would represent an unloaded, ideal system. To determine the turbine efficiency for the system, the power can be calculated based on the head and flow values given for the turbines' approximated power output compared to the theoretical output. The table below indicates the efficiency for the low-head Kaplan turbines with varying heads.

$$eff = \frac{Approx. Power}{\rho qgh}$$

In this equation, "Approx. Power" is given in the turbine specifications, ρ is the density of water, q is the volumetric flow, g is the gravity constant, and h is the specified head. Thus, the efficiency calculations are displayed in the table below.

Table 9: Low-Head Kaplan Turbine Calculations

Turbine Efficiency				
Head (ft)	Flow (GPM)	Power (W)	Approx. Power (W)	Eff
1	320	60.4	25	0.414
2	450	170	70	0.412
3	550	311	150	0.482
4	635	479	250	0.522
5	710	670	350	0.523
6	775	877	465	0.530
7	840	1110	585	0.527
8	895	1350	715	0.529
9	950	1610	850	0.527
10	1000	1890	1000	0.530

Most large hydro turbines operate at an efficiency of at least 90%. Turbines with very small head values generally function at a much lower efficiency, which explains the significantly lower efficiency calculated. The efficiency of the system for the determined head of the scaled up model can be estimated at about 40% for the low-level head, characterized by the system at about 1ft, correlating with the calculated efficiencies above. This efficiency is used in the power calculation to determine the power output of both the prototype model and full-scale operating system.

In order to optimize the power output of the wave energy converter, it is important to understand the head and flow parameters of the chosen turbine for the system as is graphed in Figure 38.

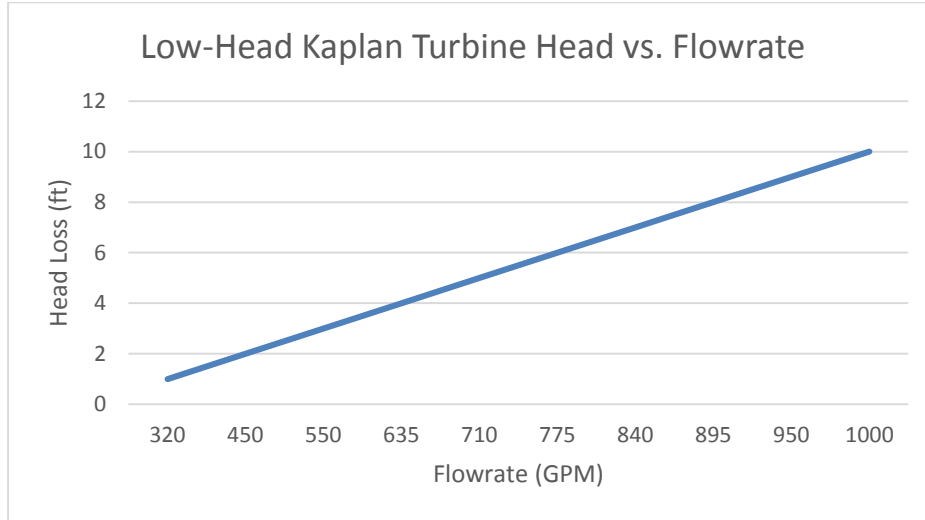


Figure 38: Low-Head Kaplan Turbine Characteristics (1000W Low Head Kaplan Turbine, 2015)

The graph represents the operating flowrate of researched Kaplan turbines that adhere to the parameters for the given head of the system. The turbines are incapable of functioning at a higher flowrate than shown in the graph; therefore, the system should be designed to operate based off the limitations illustrated in the graph. Using the maximum flowrate capacity from the low-head Kaplan turbine data, the optimal number of Kaplan turbines can be found for the system while maintaining constant head. According to the graph above, the first tier of the wave energy converter, measuring a head of 2ft, will operate at a flowrate of about 450GPM. The total flowrate for this tier can then be divided by this actual flow to determine the optimal number of turbines as displayed in Table 10. The turbine flow for the middle tier can be interpolated based on the linear graph of head vs. flowrate with a head of 1.3ft by:

$$\frac{1.3 - 1.0}{x - 320} = \frac{2 - 1}{450 - 320} \rightarrow x = 359 \text{ GPM}$$

Similarly as before, the optimal number of Kaplan turbines can be determined by dividing the calculated volumetric flowrate by the turbine operation flowrate of 359 GPM. The results for the optimal number of Kaplan turbines is summarized in the table below:

Table 10: Optimized Number of Kaplan Turbines

Tier	Full-Size Model Scale			
	Head(ft)	Volumetric Flow (GPM)	Kaplan Turbine Flow (GPM)	Number of Kaplan Turbines
Top	0.7	0.0	0.0	0.0
Middle	1.3	3802.6	359.0	11
Bottom	2.0	6769.7	450.0	15

Therefore the actual power output of the system will be the total calculated power multiplied by the number of turbines used:

Table 11: Actual Power Output of the Full-Scale System

Tier	Full-Size Model Scale		
	Calculated Power (W)/ft of Wavefront	# of Kaplan Turbines	Actual Calculated Power (W)/ft of Wavefront
Top	0.0	0	0.0
Middle	5.0	11	54.8
Bottom	13.3	15	199.4
Total	18.3	26	254.2

The overall calculated power increases due to the optimization of flow rate through the system. The low head Kaplan turbines used have a maximum operating flowrate and will be saturated at any higher speeds. Therefore, to increase the power, Table 11 displays the number of turbines that should be used and the actual power per foot of wavefront based on the optimized values. The power output is then maximized by ensuring that the flowrate through each turbine never exceeds the highest operating speed to conserve energy for the best performance.

The overall design of the proposed combined device can be compared to that of the Wave Dragon which is currently one of the top competing overtopping wave energy converters on the market. The results compare significantly in favor of the combined design to enhance efficiency while taking up much less space in the ocean.

Table 12: Proposed Design vs. Existing Market

Parameters	Sea Slot	Wave Dragon
Power Output (W)/ft of Wavefront	250	133.3
# of Kaplan Turbines	26	7
Area (ft ²)	1085	17226
Height (ft)	3.9	10.8
# of Reservoirs	3	1

Chapter 6 – Conclusions & Future Improvements

From the results presented in the last chapter, it was concluded that the combined overtopping wave energy converter proves to be a desirable product to use in the field of renewable energy. Combining the offshore location of the Wave Dragon with the multi-tiered component of the SSG, an overtopping device with superior power production capabilities was created. When compared to similar devices, the combined prototype produces more power and takes up less overall area. Placing an overtopping device in the open ocean presents some environmental concerns, but due to the location of many marine habitats on the shoreline, the environmental impact will be minimal. Since overtopping devices float on the surface of the water, there will be little interference with sea creatures' natural habitat. When scaled up to a full sized model, the combined overtopping device shows great promise in the field of wave energy harvesting.

Although this device shows successful results, there are several recommendations to improve this product further, including:

- Variation of flow diameter to optimize flowrate based on projected head loss
- Variation of wave conditions for best year-round performance
- Optimization of turbine characteristics for low-head and flowrate requirements
- Optimization of tier height and number of tiers for best collection efficiency
- Inclusion of wave reflectors to capture more wave volume and direct waves to entrance point

In addition to the design and testing tasks that should be completed in further research, an in-depth cost analysis would determine the feasibility of implementing the proposed system. There are a number of fundamental aspects that can contribute to cost efficiency including material optimization, maintenance, and power production parameters. Taking these values into consideration will then produce a cost per unit energy that can be weighed for feasibility. Due to time constraints, materials and maintenance costs were not researched in depth with a primary focus on power production. Completing further research in various aspects would establish a firmer conclusion to define the cost efficiency of the proposed system. Future developments focusing in these areas will ultimately lead to an even more efficient overtopping device, innovating the field of renewable energy.

References

- 1000W Low-Head Kaplan Hydro Turbine. (n.d.). Retrieved April 17, 2015, from <https://www.aurorapower.net/products/categoryid/4/list/1/level/a/productid/234.aspx>
- Alamian, R., Shafaghat, R., Miri, S.J., Yazdanshenas, N., Shakeri, M. (2014). Evaluation of Technologies for Harvesting Wave Energy in Caspian Sea. *Renewable and Sustainable Energy Reviews*, 32, 468-476.
- Bedard, Roger. "Offshore Wave Power Feasibility Demonstration Project." 2005.
- Biscuit Joint. (n.d.). Retrieved March 1, 2015, from <http://www.builderbill-diy-help.com/biscuit-joint.html>
- Emay, L. "Energy and the Environment-A Coastal Perspective." 22 May 2010. unc.edu. 16 October 2014 <<http://coastalenergyandenvironment.web.unc.edu/ocean-energy-generating-technologies/wave-energy/oscillating-water-column/>>.
- Esteban, M., Leary, D. (2012). Current Developments & Future Prospects of Offshore Wind and Ocean Energy. *Applied Energy*, 90, 128-136.
- Lockwood, Deirdre. "Harvesting Power When Freshwater Meets Salty." *CEN RSS*. 26 Nov. 2013. Web.
- Natesan, A. (1994). Kinematic analysis and synthesis of four-bar mechanisms for straight line couple curves. Thesis: *Rochester Institute of Technology*
- Payne, Gregory. Guidance for the experimental tank testing of wave energy converters. United Kingdom: The University of Edinburgh, 2008.
- Pelamis Wave Power. 5 June 2014. 16 October 2014 <<http://www.pelamiswave.com/our-projects/project/1/P2-Demonstration-at-EMEC-Orkney>>.
- Tester, J.W., Drake, E.M., Driscoll, M.J., Golay M.W., Peters, W.A., "Chapter 14: Ocean Wave, Tide, Current, and Thermal Energy Conversion." *Sustainable Energy*. 2nd edition, 2012, MIT Press.
- Thurman, Harold. Essentials of Oceanography. 1992.
- Vicinanza, Diego, Lucia Margheritini, Jens Peter Kofoed, and Mariano Buccino. "The SSG Wave Energy Converter: Performance, Status and Recent Developments." *Energies* 5.2 (2012): 193-226.

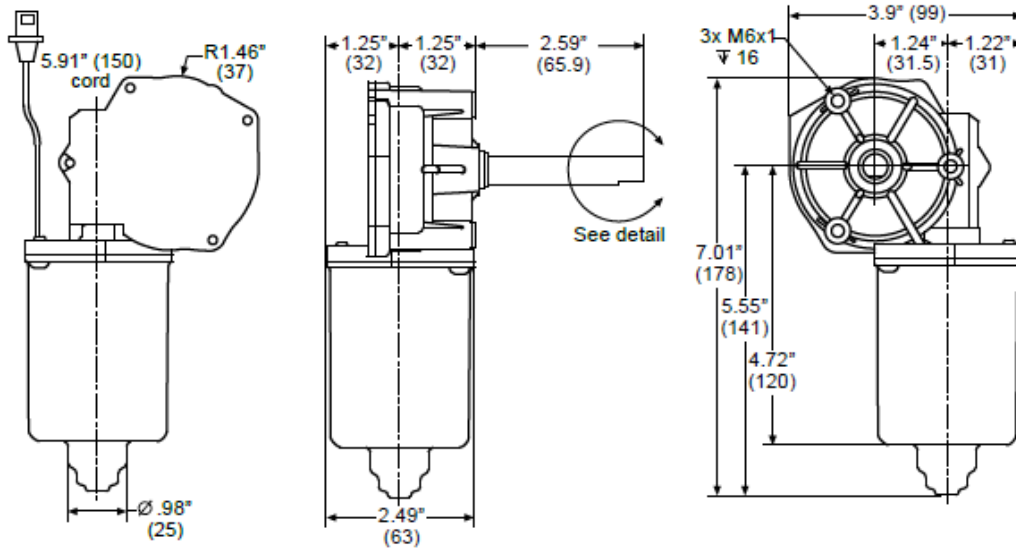
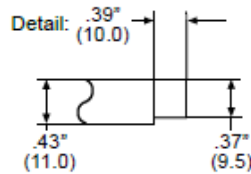
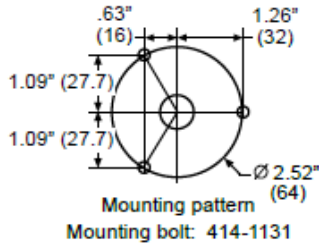
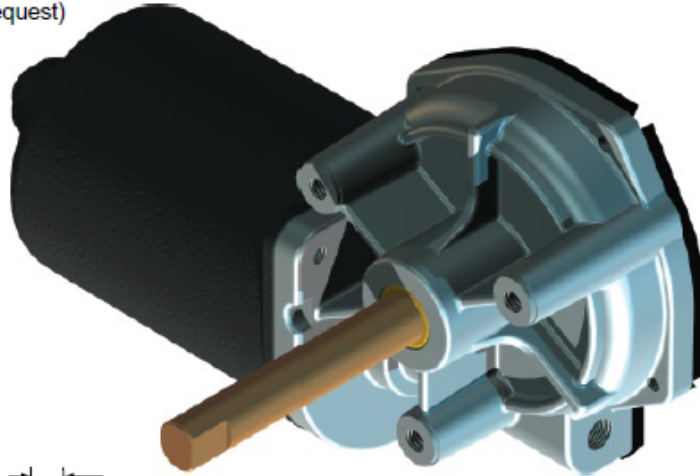
Voorhis, R. Point Absorbers: The Technology and Innovations. 25 July 2012. 16 October 2014
<<http://coastalenergyandenvironment.web.unc.edu/ocean-energy-generating-technologies/wave-energy/point-absorbers/>>.



AM EQUIPMENT.COM

226-3003 Motor

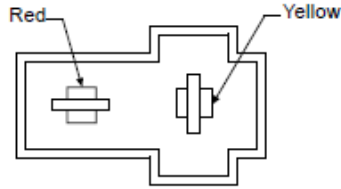
- 26Nm stall torque actuator motor. LH
- 12V reversible (24V available upon request)
- Water resistant
- For use with sprockets and drives
- Weighs 2.7 pounds



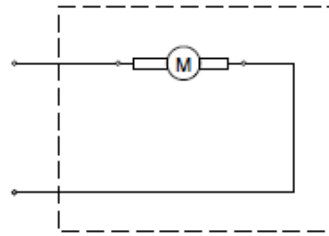
PAGE 1 OF 2



226-3003 Motor



Terminal housing: 317-1057
 Terminal: 317-1054
 Mate terminal housing: 317-1056
 Mate terminal: 317-1055



Red (+), yellow (-) = CW
 Yellow (+), red (-) = CCW (preferred rotation)

Clockwise Motor Shaft Rotation

Data Point	Data Type	Value Range
No Load	Current (A)	4.5 or less
	Speed (rpm)	95.9 - 78.5
19.5Nm	Current (A)	39.9 - 34.6
	Speed (rpm)	39.7 - 32.9
Peak Power	Power (W)	83.6 - 68.4
	Torque (Nm)	19.2 - 15.7
Nominal (Peak Efficiency)	Power (W)	44.5 nominal
	Speed (rpm)	70.2 nominal
	Current (A)	12.8 nominal
	Torque (Nm)	6.2 nominal

Counter-Clockwise Motor Shaft Rotation

Data Point	Data Type	Value Range
No Load	Current (A)	4.5 or less
	Speed (rpm)	98.1 - 80.3
19.5Nm	Current (A)	40.9 - 34.8
	Speed (rpm)	39.4 - 32.0
Peak Power	Power (W)	84.4 - 69.1
	Torque (Nm)	18.0 - 14.8
Nominal (Peak Efficiency)	Power (W)	44.1 nominal
	Speed (rpm)	74.8 nominal
	Current (A)	11.0 nominal
	Torque (Nm)	5.8 nominal

Note:
 BACKDRIVE 60Nm MINIMUM CW & CCW

